Nanoscale Advances

ROYAL SOCIETY OF CHEMISTRY

REVIEW

View Article Online
View Journal | View Issue

Cite this: *Nanoscale Adv.*, 2024, **6**, 1800

Recent progress and challenges of MOF-based nanocomposites in bioimaging, biosensing and biocarriers for drug delivery

Ngoan Thi Thao Nguyen,[abc] Thuy Thi Thanh Nguyen,[d] Shengbo Ge,[e] Rock Keey Liew,[fg] Duyen Thi Cam Nguyen*[a] and Thuan Van Tran *[a]

Metal–organic frameworks (MOFs), a burgeoning class of coordination polymers, have garnered significant attention due to their outstanding structure, porosity, and stability. They have been extensively studied in catalysis, energy storage, water harvesting, selective gas separation, and electrochemical applications. Recent advancements in post-synthetic strategies, surface functionality, and biocompatibility have expanded the application scope of MOFs, particularly in various biomedical fields. Herein, we review MOF-based nanomaterials bioimaging nanoplatforms in magnetic resonance imaging, computed tomography, and fluorescence imaging. MOFs serve as the foundation for biosensors, demonstrating efficiency in sensing H_2O_2, tumor biomarkers, microRNA, and living cancer cells. MOF-based carriers are well designed in drug delivery systems and anticancer treatment therapies. Additionally, we examine the challenges and prospects of MOFs in surface modification, release of metal ions, and interaction with intracellular components, as well as their toxicity and long-term effects.

Received 3rd December 2023
Accepted 24th January 2024

DOI: 10.1039/d3na01075a

rsc.li/nanoscale-advances

1. Introduction

The biomedical field has long been a priority, driven by the ongoing interest in health information and the advancement of healthcare.[1] It is crucial for new technologies to continuously evolve in response to the persistent threats posed by human diseases. Therapeutic agents face common limitations, including low bioavailability, severe adverse effects, and rapid elimination from the body.[2] This has prompted the material technologies to exploit and apply solutions within the realms of disease treatment and diagnosis. Over the past two decades, the biomedical materials sector has rapidly progressed, offering remedies for defect repair, deformity correction, tissue replacement, and efficient therapeutic delivery.[3] Such a trend has notably contributed to an increased average life expectancy in developed countries.

When delving into materials technology for biomedical applications, researchers have developed an array of nanoparticles using diverse synthetic platforms.[4–6] These nanoparticles, owing to their minute size and heightened sensitivity, serve as valuable contrast agents.[7] Moreover, they can be harnessed for coupling with targeting ligands or in combination with functional agents, making them apt for bioimaging applications.[8] Notably, various forms of nanoparticles—polymeric nanoparticles, polymeric micelles, magnetic nanoparticles, liposomes, and dendrimers—have been successfully created.[9] Some studies even showcase their direct efficacy in eradicating cancer cells or exhibiting antibacterial and anti-inflammatory properties.[10–12] However, nanomaterials come with limitations pertaining to toxicity, biological stability, drug loading capacity, and other characteristics, inhibiting their transformation into radical materials for multifunctional and intricate therapeutic applications. In this context, metal–organic frameworks (MOFs) emerge as a novel class of porous materials composed of metal-containing nodes and organic bonding.[13] Since their inception, MOFs created through the amalgamation of metal ions or clusters with organic bonds have garnered immense attention.[14] Typical cage-like MOFs boast numerous recurring bonds facilitated by metal ions serving as binding nodes alongside organic ligands. Metal ions (*e.g.*, Zn, Ca, Zr, Mg, and Cs) are often used together with organic linkages such as phosphonates, carboxylates, and sulfonates to

[a]*Institute of Applied Technology and Sustainable Development, Nguyen Tat Thanh University, 298-300A Nguyen Tat Thanh, District 4, Ho Chi Minh City 755414, Vietnam. E-mail: ntcduyen@ntt.edu.vn; tranuv@gmail.com; tranvt@ntt.edu.vn*

[b]*Faculty of Chemical Engineering, Ho Chi Minh City University of Technology (HCMUT), 268 Ly Thuong Kiet Street, District 10, Ho Chi Minh City, Vietnam*

[c]*Vietnam National University Ho Chi Minh City, Linh Trung Ward, Thu Duc District, Ho Chi Minh City, Vietnam*

[d]*Department of Chemical Engineering and Processing, Nong Lam University, Thu Duc District, Ho Chi Minh City 700000, Vietnam*

[e]*Co-Innovation Center of Efficient Processing and Utilization of Forest Resources, College of Materials Science and Engineering, Nanjing Forestry University, Nanjing, 210037, China*

[f]*Higher Institution Centre of Excellence (HICoE), Institute of Tropical Aquaculture and Fisheries (AKUATROP), Universiti Malaysia Terengganu, 21030, Kuala Nerus, Terengganu, Malaysia*

[g]*NV Western PLT, No. 208B, Second Floor, Macalister Road, Georgetown, 10400, Penang, Malaysia*

form MOFs.[15] They exhibit versatility as gas storage,[16] purification[17] and separation platforms, porous photocatalysts,[18] cargo delivery systems,[19] sensors,[20] and energy-related applications like supercapacitors and energy converters.[21] Due to their remarkable capability to modulate the structure and function, MOFs stand out as one of the fastest-expanding fields within biomedical materials technology.[23–25]

The properties of MOFs, such as high porosity, a large surface area, ample pore size, biocompatibility, and ease of post-synthesis modification, render them promising alternatives in biomedicine.[26] Positive agents can be introduced into MOFs through two primary methods: integrating functional agents into the framework or loading them into the pores.[27] MOFs offer flexibility in leveraging both metal clusters and their ligands for diagnostic imaging and disease treatment. For example, Kong *et al.*[28] synthesized the green-emitting BUT-88 material generated from a suitable luminescent tetracarbazolyl octa-carboxylate ligand, demonstrating its application in the fluorescence diagnostic technique for detecting microRNA-21. Similarly, Chakraborty *et al.*[29] utilized a tetradentate phosphonate ligand to synthesize Cu-MOF, which acted as a fluorescent agent to enhance cancer therapy through light irradiation.

With the advancement of synthesis processes and the development of new technologies, there is a demand for designing and manufacturing MOFs with controlled and enhanced structural properties, including pore size, particle diameter, and pore volume.[30] Various methods have been employed for synthesizing MOFs, including hydrogen/solvothermal synthesis,[31,32] microwave and ultrasonic assisted synthesis,[33,34] mechanochemical synthesis,[35] electrochemical synthesis,[36] spray drying synthesis,[37] and solvent evaporation.[38] However, these approaches pose challenges related to production scale, synthesis efficiency, and physicochemical quality, among others. Among these methods, the hydrothermal approach stands out as particularly popular due to its ease of preparation and straightforward synthesis.[39] For example, Hao *et al.*[40] utilized the hydrothermal method to synthesize the MWCNT/Ni–Mn–S material at high temperature and pressure, tailored for electrochemical energy storage applications. The resulting material demonstrated high specific capacitance and excellent cycling stability. Additionally, the solvothermal method has gained significant traction in numerous studies. Similar to the hydrothermal technique, it operates within a closed environment at high temperature and pressure but uses a solution devoid of water.[41] In the photocatalytic study, Shi *et al.*[42] developed ZnFe-MOF composites by incorporating Bi^{3+} through a solvothermal process. The optimal BiOBr@ZnFe-MOF showed high removal efficiency for tetracycline and rhodamine B under visible light. However, these methods often demand extended reaction times, organic solvents, and harsh conditions like high temperatures and pressures, making them energy-intensive and unsuitable for large-scale production. Alternatively, microwave-assisted synthesis has emerged as a promising approach to enhance MOF production, increasing pore volume and ensuring uniform size distribution while reducing synthesis time. This method offers accelerated reaction speed, higher yield, greater selectivity, and cost-effectiveness for synthesizing various MOFs.[43] Consequently, many studies have shifted from conventional heating to microwave-assisted methods.[44] Indeed, Bazzi *et al.*[45] employed ultrasonic and microwave methods to synthesize the ZIF-8 material for phosphate adsorption. They demonstrated the conversion of zinc oxide to ZIF-8 under microwave and ultrasonic irradiation using different solvent mixtures such as dimethylformamide/water, methanol/water, and water. Synthetic MOFs have exhibited remarkable adsorption potential, paving the way for developing MOFs from sustainable inorganic sources through microwave-assisted synthesis. Additionally, methods like spray drying, electrochemical processes, or solvent evaporation prove effectiveness in synthesizing MOFs for drug delivery applications. Overall, understanding the impact of particle size, morphology, and functionality on the intended use of MOFs is crucial to identify the most suitable synthesis method for biomedical applications.

In the realm of biomedical applications, several challenges of MOFs require focused attention, notably the precise control of particle size and porosity alongside understanding their metabolic behavior *in vivo*. Biocompatibility and effective binding capacity for cargo loading are crucial considerations.[46] Diverse surface functionalization strategies hold promise in enhancing MOFs for physiological stability, controlled cargo release, and specific target recognition.[47] These strategies aim to bolster catalytic reactivity and extend circulation within the body, minimizing immune reactions or premature elimination. The properties of the developed MOF can have two modes of functionalization: by using a combination of organic compounds and metal-containing nodes or by functionalizing the surface post-synthesis.[48] Usually, the post-synthetic functionalization method is used to easily add other functional compounds to MOFs. Post-synthetic functionalization is commonly favored as it allows for easy addition of other functional compounds to MOFs. Compounds employed for surface functionalization, capable of conjugating to organic ligand groups through covalent or strong coordination, include –COOH, $–NH_2$, $–N_3$, *etc.*, as well as metal nodes on the surface of MOFs. For instance, Liu *et al.*[49] conducted a synthesis of the Ni-MOF material for the development of a luminescent detector targeting aspartic acid. To leverage the high porosity of the MOF, they introduced photoactive Eu^{3+} ions using a simple embedding method, resulting in Eu^{3+} functionalized MOFs. To enhance physiological stability and diminish immunoreactivity, MOFs are functionalized with polymer like liposomes and polyethylene glycol. Gupta *et al.*[50] explored the synthesis of UiO-66 coated with a biocompatible polyethylene glycol layer, noting that UiO-66/polyethylene glycol extended drug release duration. Moreover, in biomedical applications, MOFs consistently demonstrate significant potential due to their adaptability for modification and functionalization, which enhances application efficiency. Functionalized MOFs commonly exhibit improved outcomes compared to non-functionalized counterparts. Indeed, Paiman *et al.*[51] synthesized Fe-MOF and functionalized the amine using different

organic linkages of 2-aminoterephthalic acid. The functionalization demonstrated a remarkable effect: the amine-Fe-MOF exhibited a two-fold higher adsorption capacity despite being loaded at half the quantity compared to the non-functionalized Fe-MOF.

Recent studies have extensively explored synthesis strategies and potential applications of MOFs in biomedicine. However, the existing reviews only covered several selected aspects, leaving many unaddressed categories. For example, Moharramnejad *et al.*[52] discussed modifying MOFs for biomedical technologies like drug delivery but did not delve into other potential applications. In another study, Xu *et al.*[53] demonstrated the biomedical potential of MOFs in therapeutic pathways without exploring disease diagnosis thoroughly. Similarly, Fatima *et al.*[54] mentioned various stimuli-responsive MOFs for targeted drug delivery but many promising biomedical applications were not encompassed. Motivated by these gaps, here, we present a comprehensive review focusing on MOFs in early disease diagnosis, specifically in sensing and bio-imaging pathways. Furthermore, we clarify the role of MOFs in drug transport *via* blood, oral routes, skin, and eyes. Through detailed examinations, the significant contributions of MOFs in advancing biomedical technology are highlighted.

The graphical representation in Fig. 1a demonstrates the interconnections among keywords like metal–organic framework, biomedical applications, drug carrier, controlled drug delivery, drug effect, animals, diagnostic imaging, *etc.*, highlighting their strongest linkages. The trend over a 10-year period between 2012 and 2022 in Fig. 1b shows an increasing research interest in the field of metal–organic frameworks for biomedical applications. In 2012, there were merely five publications on this topic, but by 2021, this number peaked at 199 studies. The total citation counts also surged from 875 in 2012 to an impressive 10 837 citations by 2022. This growth signifies a widespread dissemination of knowledge and a profound surge in interest regarding the biomedical applications of MOF-based materials in recent years.

2. MOF-based bioimaging nanoplatforms

2.1. Magnetic resonance imaging

MOFs have emerged as potential candidates for biomedical applications, particularly as novel magnetic resonance imaging (MRI) contrast agents. The technique of MRI, due to its contrast mechanisms, has become a highly adaptable imaging modality in routine clinical assessments.[55] Considering the human body consisting of approximately 70% water, leveraging the magnetism of hydrogen atoms with water in the body enables the recording of distinct water distribution in tissues. Pathological injuries often cause alterations in water distribution at the injury site compared to normal tissue, facilitating the identification and detection of tumors and diseases.[56] MRI relies on the interaction between an external magnetic field and hydrogen atoms within soft tissues, providing high spatial resolution images.[57] The image signal depends on the longitudinal (T_1) and transverse (T_2) relaxation rates of water protons, represented inversely as the relaxation rates R_1 and R_2 along vertical and horizontal axes.[58] Recent advancements involve the use of various MOFs containing Mn, Gd, Fe, and their derivatives to develop high-resolution MRI effects as contrast agents. These MOFs can serve as carriers for MRI contrast agents such as gadolinium, iron platinum, and iodine-containing contrast materials for bioimaging applications.[59] The appeal of MOF materials in MRI is their versatility, attributed to their composition of metal ions, large pore width, and expansive surface area, enabling multifaceted applications (Fig. 2a). Firstly, MOFs effectively and safely deliver *in vivo* contrast agents or utilize metal ions within their framework. Secondly, they load photosensitizers for simultaneous applications in photoacoustic and photothermal imaging. Thirdly, MOFs act as drug carriers for both diagnosis and targeted drug release. Consequently, MOFs have demonstrated their potential, convenience, and versatility in imaging techniques and cancer treatments.

Jia *et al.*[60] synthesized Gd/DTPA/MOF-808/PANI (Gd(III) combined with diethylenetriamine pentaacetate, DTPA, and polyaniline, PANI) for magnetic resonance bioimaging of 4T1

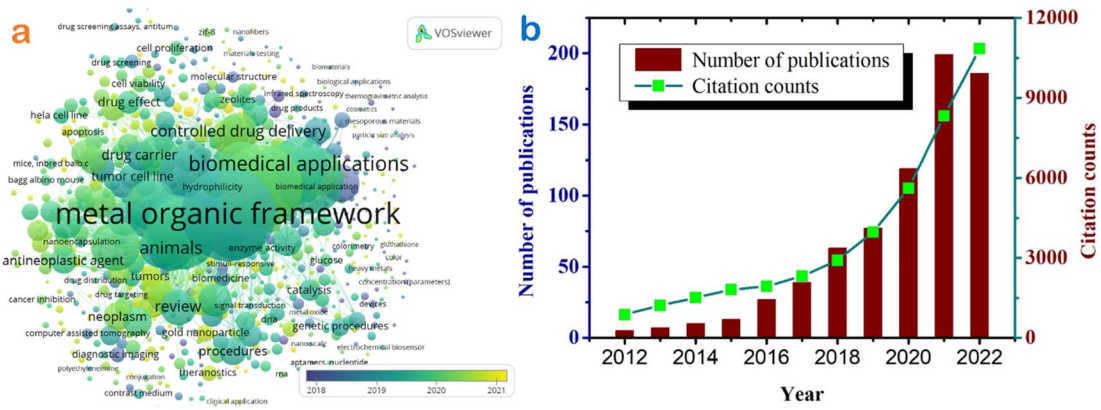

Fig. 1 A bibliometric analysis using VOSviewer software (a) and the number of publications reported on MOFs (b). Data retrieved from Scopus with keywords as "metal–organic framework" and "biomedical" between 2012 and 2022. Bibliometric pattern.

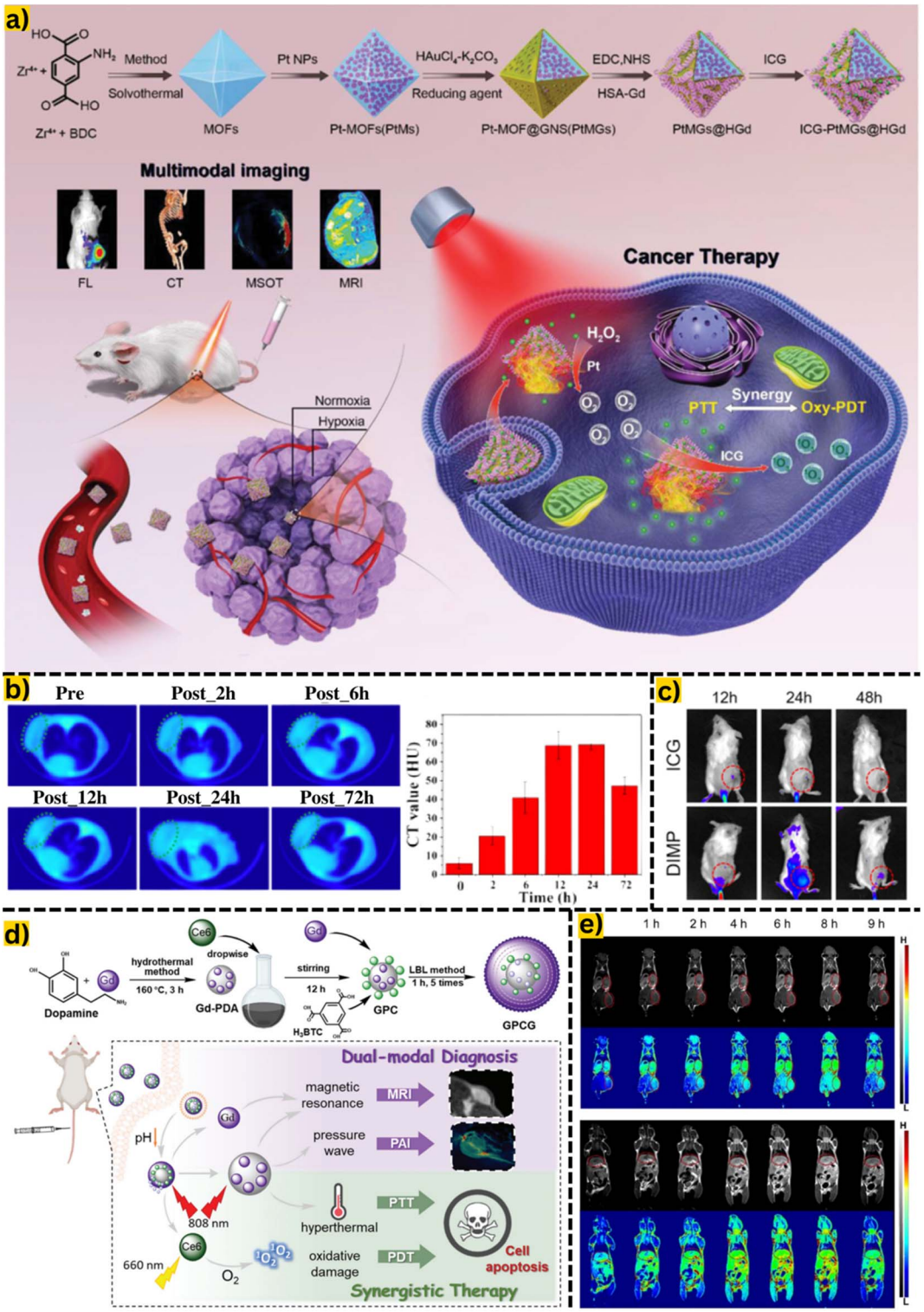

Fig. 2 (a) Detailed synthesis of MOFs from Zr^{4+} and benzene-1,4-dicarboxylic acid by a solvothermal method and post-synthesis modification by loading indocyanine green. Reproduced from ref. 63 with permission from Wiley-VCH Verlag, copyright 2020. (b) Tumor computed tomography images of mice after intravenous injection of the material at different time intervals (2, 6, 12, 24, and 72 h) are denoted by a green dashed ellipse. Computed tomography value (HU) of the material after each time interval. Reproduced from ref. 64 with permission from Dove Medical Press Ltd, copyright 2020. (c) Fluorescence images of 4T1 tumor-bearing mice injected with indocyanine green and intracellular acidity-responsive polymeric MOF nanoparticles at different time points, tumors marked with red circles. Reproduced from ref. 65 with permission from Elsevier, copyright 2021. (d) Phototherapy and synergistic treatment based on a single MOF material, Gd-MOF. Specifically, Gd from the MOF can support magnetic resonance imaging and Gd-polydopamine increases pressure waves for photothermal imaging application. In addition, loading chlorine6 onto the MOF surface also supports increased hyperthermal and oxidative damage to photothermal and photothermal therapies. Reproduced from ref. 66 with permission from the Royal Society of Chemistry, copyright 2021. (e) Magnetic resonance images on the

breast cancer cells. The obtained results indicated an R_1 elongation of 30.1 mM^{-1} s^{-1} (0.5 T). Notably, the R_1 value of Magnevist, a commercial contrast agent, was significantly lower than that of MOF-based bioimaging, affirming the potential of MOF materials in diagnostic imaging. Interestingly, Zhu *et al.*[61] showed the synthesis of Fe-DOX@Gd-MOF-ICG (doxorubicin, DOX; indocyanine green, ICG) using Gd^{3+} as a magnetic resonance imaging contrast agent. They successfully employed photoacoustic and photothermal imaging methods on an imaging platform by loading the indocyanine green photosensitive agent into the MOF. The findings revealed R_1 of 6.4 mM^{-1} s^{-1} and R_2 of 81.9 mM^{-1} s^{-1}. Based on magnetic resonance imaging diagnosis results, MOFs continued to be used for photoacoustic and photothermal imaging therapy, significantly contributing to MOF-based nano-hybrid materials in MRI, as well as effective photoacoustic and photothermal imaging. In another study, Pandit *et al.*[62] developed Fe_3O_4@-ZIF8@ZIF67@folic acid by decorating ZIF-8@ZIF-67 with Fe_3O_4 nanoparticles and folic acid to guide precise chemotherapy of MCF-7 breast cancer cells *via* magnetic resonance imaging. They achieved higher R_1 and R_2 relaxivity values (2.042 and 85.86 mM^{-1} s^{-1}) than the study conducted by Zhu *et al.*[61] This enhancement was attributed to the effectiveness of iron oxide doped in MOFs as magnetic support and contrast agents, confirming contrast improvement with increased iron oxide concentration.

2.2. Computed tomography

Computed tomography (CT) is a diagnostic technique utilizing multiple X-rays to scan cross-sectional areas of the body, aiding in disease diagnosis.[67] Contrast agents within the body interact with X-rays, generating image signals that render affected lesion structures bright white, distinguishing them from normal tissue. Notably, elements with high atomic numbers (Z) tend to attenuate X-rays, enhancing X-ray irradiance.[68] Currently, the use of high X-ray attenuation contrast agents, such as iodine and barium, is restricted due to their rapid clearance rates and high dosage requirements. However, recently discovered MOFs show promise as contrast agents, offering high intensity with minimal drawbacks.

Bao *et al.*[64] recently synthesized Hf/Mn-TCPP-MOF (TCPP, 4,4,4,4-(porphine-5,10,15,20-tetrayl)tetrakis) using Hf^{4+} clusters and MnH_2-TCPP ligands as a contrast agent for computed tomography (CT) imaging. Due to its high X-ray attenuation capacity, Hf ($Z = 72$) demonstrates the potential for sensitive CT scanning and is being considered as a contrast agent. Reported results indicated that the CT value of the MOF (70 HU) was 1.7 times higher than that of iohexol, a commercial contrast agent, as shown in Fig. 2b. In a study by Ma *et al.*,[69] the NMOF545@Pt synthesized from $HfCl_4$, Mn-TCPP, and H_2PtCl_6 exhibited a CT value of 110 HU, surpassing the MOF synthesized by Bao *et al.*[64] The higher concentration of Pt ($Z = 78$) in this study may influence signal enhancement in CT. Additionally, this study highlights NMOF545/Pt as a potential contrast agent for MRI/CT/PAI imaging modalities, showcasing its promising role in diagnostic imaging technology. Similarly, You *et al.*[63] fabricated a MOF-based therapeutic system integrating modalities such as CT, MRI, and FL for precise cancer chemotherapy. These MOFs were constructed using 2-aminoterephthalic acid (NH_2-BDC) ligands and Zr^{4+} metal nodes, modified with Au^+ and Pt^+. Interestingly, the authors observed that increasing the concentration of Au on the MOF resulted in progressively brighter CT images, showing a notable linear relationship. This improvement is attributed to the presence of octahedral gold nanoshells ($Z = 79$), significantly enhancing the reflective properties of the MOF materials.

2.3. Fluorescence imaging

Fluorescence imaging (FL) is a non-invasive imaging technique utilized to visualize biological processes within living organisms. Fluorescence, a form of luminescence, is triggered when materials emit light of a specific wavelength after absorbing electromagnetic radiation.[70] Molecules exhibiting this light-emitting property upon light absorption are known as fluorophores.[71] FL is widely employed due to its high sensitivity, exceptional resolution, and user-friendly operation. MOFs are materials synthesized from ligands and metal frameworks, characterized by their large pore structures. They can efficiently host fluorescent agents for imaging purposes or utilize their own luminescent ligands directly Table 1.

For example, Wang *et al.*[72] utilized Zr^{4+} and H_2L as organic ligands to create MOFs with near-infrared fluorescence properties capable of producing singlet oxygen. The study focused on detecting liver tumors in mice by injecting MOFs into the body and observing the resulting fluorescence images. Areas exhibiting high intensity in red indicated mouse tumors, which persisted for up to 72 h post-injection. Additionally, MOFs functioned as carriers for fluorescent compounds, such as the commonly used contrast agent in FL imaging, indocyanine green. Indeed, Zhang *et al.*[65] reported MOF@ICG@DOX, derived from Zn^{2+} and 2-methylimidazole, with ICG loaded into MOF pores for PTT and FL imaging. As observed, the fluorescent material primarily concentrated at the tumor site 12 h post-injection and gradually spread throughout the body after 24 h as shown in Fig. 2c. However, the means of eliminating MOFs carrying ICG from the body, likely through urine after 24 h, was not addressed. Further research is necessary to understand the fate of MOFs post their function in the body and the elimination

coronary plane of 4T1 mice in different stages after injection of MOF-based materials at tumor sites, liver and kidney. Tumors are marked with red circles. Reproduced from ref. 60 with permission from the Royal Society of Chemistry, copyright 2021. Abbreviations: benzene-1,4-dicarboxylic acid, BDC; fluorescence imaging, FL; computed tomography, CT; multi-spectral optoacoustic tomography, MSOT; magnetic resonance imaging, MRI; intracellular acidity-responsive polymeric MOF nanoparticle, DIMP; photothermal therapy, PTT; photodynamic therapy, PDT; indocyanine green, ICG; photoacoustic imaging, PAI; photothermal imaging, PTI; multifunctional Gd-PDA-Ce6@Gd-MOF, GPCG; polydopamine, DPA.

Table 1 Recent progress in MOF-based nanocomposites in bioimaging applications

No.	MOFs	MOF skeleton components	Imaging agent	Imaging strategy	Application	References
1	Au@Fe(BTC)$_3$(H$_2$O)$_6$	Au^{2+} and Fe(BTC)$_3$	Au	MRI, NIR (R_2 = 61.57 mM s^{-1} at 1 T)	MDA-MB-23, MCF-7, 5637, RT112	186
2	Gd-DTPA-MOF-808@PANI	Zr^{4+} and DTPA	Gd^{3+}	MRI (R_1 relaxivity of 30.1 mM^{-1} s^{-1} at 0.5 T)	HUVEC, 4T1 cells	60
3	MIL-100(Fe)	Fe^{3+} and ammonium thiocyanate	MIL-100(Fe)	Label for MRI (loading dotarem)	—	187
				R_2 = 4.0 mM^{-1} s^{-1} at 1.5 T		
4	H_2L-MOF	Zr^{4+} and H_2L	H_2L, DOX	FLI	HeLa	72
5	UiO-66(Zr)-(COOH)$_2$ MOFs	Zr^{4+} and H_4BTeC	Mn^{2+}, DOX	MRI	HUVEC, 4T1 cells	188
6	Fe$_3$O$_4$@ZIF8@ZIF67@folic acid	Co^{2+} and 2-MeIM	Fe$_3$O$_4$	MRI	MCF-7	62
				R_1 = 2.042 mM^{-1} s^{-1}		
				R_2 = 85.86 mM^{-1} s^{-1}		
7	Fe-DOX@Gd-MOF-ICG	Gd^{3+} and H_3BTC	Gd^{3+}, DOX	MRI/PAI/PTI	4T1	61
				R_1 = 6.4 mM^{-1} s^{-1} and R_2 = 81.9 mM^{-1} s^{-1}		
8	Hf/Mn-TCPP-MOF	$HfCl_4$ and MnH$_2$-TCPP	fHMNM, Hf_6	MRI/PAI/PTT/CT	4T1, HeLa	64
9	Gd-PDA-Ce6@Gd-MOF	Gd^{3+} and H_3BTC	Gd^{3+}, Ce6	MRI/PAI/PTT/PDT	4T1	66
10	MIL-100(Fe)	—	MIL-100(Fe)	PAI/MRI	Y79	189
11	Fe$_3$O$_4$@MOF-DOX-CDs-Apt	Zr^{4+} and NH$_2$-BDC	Carbon, Fe$_3$O$_4$	FLI	MDA-MB-231	190
12	NMOF545@Pt	$HfCl_4$ and Mn-TCPP	Pt, hafnium, Mn	CT/MRI/PAI	4T1	69
13	DOX-Gd-TCPP	Gd^{3+} and TCPP	DOX, Gd^{3+}	MRI/FL	4T1	73
14	MOF@ICG@DOX	Zn^{2+} and 2-methylimidazole	Indocyanine green	PA/IR/FL	4T1	65
15	ICG-PtMGs@HGd	Zr^{4+} and NH$_2$-BDC	Au, indocyanine green	FL/CT/MSOT/MRI	4T1	63
16	Gd-DTPA@ZIF-8	Gd^{3+} and 2-methylimidazole	ZIF-8, Gd^{3+}	MRI	HUVEC, 4T1 cells	191

mechanism to ensure safety. In another instance, Yuan *et al.*[73] proposed a fluorescent probe, DOX-Gd-TCPP-MOF, for diagnosing 4T1 cells. The DOX-loaded MOF demonstrated potential for anti-tumor therapy and fluorescence treatment in FL imaging. Recent studies have also showcased the potential to construct efficient and rapid MOF-based multimodal imaging platforms for *in vivo* tumor imaging (Table 2). These advancements underscore MOFs as a versatile material for future testing and diagnostic engineering in various applications.

3. MOF-based biosensors

Traditional cancer diagnostic techniques such as X-ray, positron emission tomography (PET), ultrasound, computed tomography (CT), and magnetic resonance imaging (MRI) have significantly advanced early cancer detection.[74] However, these methods often lack the required sensitivity and specificity for precise clinical diagnosis. Consequently, this limitation may lead to incorrect diagnoses or the inability to initiate optimal treatment at the most opportune time.[75] Therefore, there has been a concerted effort to explore molecular biology-level diagnostic methods. MOFs have emerged as promising tools for disease diagnosis and early sensing. Various types of MOF-based biosensors have been developed to detect reactive oxygen species,[76] cancerous tumor markers,[77] microRNAs (miRNAs),[28] and living cancer cells,[78] as shown in Table 3. These biomarkers are recognized as common indicators for early cancer detection and screening for the initial spread of tumors. Leveraging the extensive surface area and high stability of MOFs, these MOF-based biosensors demonstrate exceptional sensing capabilities with low detection limits. This section aims to explore and elucidate the biological and potential applications of MOF-based biosensors.

3.1. H_2O_2 sensing

H_2O_2 serves as a crucial micronutrient, significantly contributing to various human physiological processes. Disruptions in H_2O_2 levels can lead to oxidative stress, accelerating aging and fostering various serious ailments such as Alzheimer's disease, cardiovascular disorders, and cancer.[79,80] Consequently, the development of a dependable and efficient method to real-time monitor H_2O_2 secretion from living cells is imperative. The direct diffusion of molecules into the pores of MOFs can serve as the basis for immobilizing enzymes and other molecules in electrochemical sensors.[81] Employing a sensor platform utilizing MOF-loaded materials holds significant promise for biomedical monitoring applications.

In recent studies, there has been a growing exploration of MOF applications in biosensors for H_2O_2 detection. Mathew *et al.*[82] developed an electrochemical Ag–Bi-BDC(s)MOF-based biosensor for detecting H_2O_2 in THP-1 (leukemia monocytic cell) and AtT-20 cells (the pituitary gland cell of mice), achieving a limit of detection (LOD) of 0.0201 μM. The resistance of the sensor was evaluated using various interfering agents such as uric acid, dopamine, L-cysteine, and ascorbic acid, demonstrating a 95% retention of its original activity. In the same trend, Li

Table 2 Recent progress in MOF-based biosensors

No.	MOFs	MOF components	Targeting	Detection method	Detection range	Limit of detection	References
1	Cr-MOF@CoPc	Cr^{3+} and H_2BDC	CT26 cells	EIS	50–1.0 × 10^7 cells mL^{-1}	31 cells mL^{-1}	78
2	MOF Bi-TCBPE	Bi^{3+} and H_4TCBPE	Fe^{3+} in serum	Fluorescence	0–25 μM	1 μM	192
3	BODIPY@Eu-MOF	Eu^{3+} and BBDC	F^-, H_2O_2 and glucose (from HeLa cells)	Fluorescence	F^-: 0–30 μM, H_2O_2: 0–6 μM Glucose: 0–6 μM	F^-: 0.1737 μM, H_2O_2: 0.0062 μM Glucose: 6.92 nM	83
4	MOF-derived N-doped porous carbon	Mg^{2+} and PVP	Acetylcholinesterase (cholinesterase cause Alzheimer and Parkinson)	Colorimetric assay	0–5 U L^-	0.0001 U L^{-1}	86
5	Zn-MOF/GO	Zn^{2+} and TCPP	p53 antibody	Combined p53 antigens	0.1 fg mL^{-1}–0.01 ng mL^{-1}	0.03 fg mL^{-1}	193
6	Graphdiyne/Ru@MOF@NCNDs-Ru	Zn^{2+} and 2-NH_2-BDC	CA19-9 (tumor marker)	ECL	0.0005–200 U mL^{-1}	0.00013 U mL^{-1}	91
7	drDNA-BUT-88	Zr^{4+} and TCTA	microRNA-21	Fluorescence	0.2–1.0 nM	0.13 nM	28
8	Co–Ni–Cu-MOF	Co^{2+}, Ni^{2+}, Cu^{2+}, and H_2BDC	Nilutamide (anticancer drug)	EIS	0.5–900 μM	0.48 μM	194
9	Eu-MOF	Eu^{3+}, NH_2–H_2BDC and Phen	CA242 (tumor marker)	ECL	0.005–100 U L^-	0.0019 U L^-	94
10	Pep/Au/Cu-MOF/SWNH	Cu^{2+} and benzene-1,3,5-tricarboxylic acid	Neutrophil gelatinase-associated lipocalin (biomarker of acute kidney injury)	SWV	0.00001–10 ng mL^{-1}	0.0405 pg mL^{-1}	195
11	MOF-808	Zr^{4+} and trimesic acid	CA125 (antigen – ovarian cancer biomarker)	EIS	0.001–30 ng mL^{-1}	0.5 pg mL^{-1}	92
12	Zr-MOF	Zr^{4+} and 1,4-benzenedicarboxylic acid	miRNA-15	ICDSE	1–1 × 10^6 fM	2.03 fM	103
13	MIL-125-NH_2	Ti^{4+} and 2-aminoterephthalic acid	CLD7 (colorectal cancer biomarker)	Microfluidic amperometric immunosensor	2–1000 pg mL^{-1}	0.1 pg mL^{-1}	93
14	AuNPs@Zn-MOF	Zn^{2+} and [BDBMBCIm]Cl	Alpha-fetoprotein (hepatocellular carcinoma)	PEC	0.005–15.0 ng mL^{-1}	1.88 pg mL^{-1}	90
15	HRP@Fe-MOF	—	Amyloid-β oligomer (cause Alzheimer)	Using horseradish peroxidase	0.0001–10 nM	0.03 pM	196
16	Au-NPs/Cu-HHTP-NSs	Cu^{2+} and sodium dodecyl sulfate	H_2O_2 (from colon cells SW-48)	EIS	50 nM–16.4 mM	0.0056 μM	84
17	Cu-MOF	Cu^{2+} and 1,3,5-benzenetricarboxylic acid	H_2O_2, and H_2S	Colorimetric assay	H_2O_2: 50 nM to 500 μM $Cr_2O_7^{2-}$: 50 nM to 0.5 μM H_2S: 1 nM to 0.2 μM	H_2O_2: 25 nM $Cr_2O_7^{2-}$: 30 nM H_2S: 0.2 nM	76
18	ZIF-67-Au@Pt	Co^{2+} and 2-methylimidazole	H_2O_2 (from RAW 264)	Electrochemical technology	0.8–3000 μM	0.086 μM	81
19	Ag–Bi-BDC (s) MOF	Bi^+ and BDC	H_2O_2 (from THP-1 and AtT-20 cells)	Electrochemical technology	10 μM–145 mM	0.0201 μM	82
20	ZIF-8	Zn^{2+} and 2-methylimidazole	H_2O_2 (from H9C2 and HeLa cells)	EIS	5.0 μM to 70 mM	1.67 μM	112

Table 2 (*Contd.*)

No.	MOFs	MOF components	Targeting	Detection method	Detection range	Limit of detection	References
21	MOF-818	Zr^{4+}, Cu^{2+}, and H_2PyC	H_2O_2, H_2S (from HeLa cells)	Colorimetric and electrochemical assay	H_2O_2: 0.0133–10 mM H_2S: 3–333 μM	H_2O_2: 9.02 μM H_2S: 0.8 μM	104
22	QZIF-67-2	Co^{2+} and 2-methylimidazole	H_2O_2 (from HepG2)	Electrochemical technology	2 μM–65 mM	1.2 μM	197
23	Ag@ZIF-67	Co^{2+} and 2-methylimidazole	Carcinoembryonic antigen	Chemiluminescence aptasensor	0.0001–5 ng mL^{-1}	4.53×10^{-3} ng mL^{-1}	95
24	Co-MOF-ABEI/$Ti_3C_2T_x$	Co^{2+} and ABEI	miRNA-21	ECL	0.00001–10 nM	3.7 fM	102
25	UiO-66-$2NH_2$	Zr^{4+} and 2,5-diaminoterephthalic acid	MCF-7	EIS	100–100000 cell mL^{-1}	31 cell mL^{-1}	111

et al.[83] proposed a fluorescent probe based on Eu-MOF with the BODIPY photosensitizer (5R@Eu-MOF) for H_2O_2 detection in HeLa cells. 5R@Eu-MOF exploited a unique nucleophilic reaction between the boric group and H_2O_2, altering energy transfer and enhancing light emission. This MOF-based biosensor exhibited rapid response and achieved a detection limit of 0.0062 μM within a range of 0–6 μM. In comparison, Huang *et al.*[84] reported an Au@Cu-MOF-base biosensor to detect H_2O_2 from colon cells (SW-48) using electrochemical impedance spectroscopy. The synergistic contribution of Cu-HHTP-NS and Au-NP in the composites led to distinctive electrical and structural properties, achieving a relatively low LOD of 0.0056 μM. To achieve this result, the electrochemical spectroscopy method was used for the first time based on ultrathin 2D conductive Cu-MOF nanosheets. Accordingly, Au nanoparticles are attached to the surface of MOF nanosheets with outstanding charge mobility and high electrochemical reactivity. At this time, Au-NP/Cu-HHTP-NS has a high electrocatalytic activity for H_2O_2 to dissociate into two $^{\bullet}OH$ species. As is known, the essence of electrochemical spectroscopy is to convert biochemical events into electrical signals. Consequently, the interaction process that occurs between H_2O_2 and the resulting material is shown using a measured electrical signal. These studies collectively showcase the potential of MOF-based biosensors, demonstrating wide detection ranges and exceptional accuracy in detecting H_2O_2.

3.2. Tumor biomarkers

Biomarkers serve as crucial indicators of biological processes, playing a vital role in disease detection. Tumor biomarkers, in particular, are extensively utilized for diagnosing and prognosticating various diseases, notably cancer. Enzyme activity-related tumor markers, such as adenosine triphosphate (ATP),[85] acetylcholinesterase,[86] protein tyrosine kinase-7 (PTK7),[87] lymphocyte activation protein gene-3 (LAG-3),[88] nuclear matrix protein-22 (NMP-22),[89] and α-fetoprotein (AFP),[90] are commonly studied. Disease-specific antigens, including carbohydrate antigen 19-9 (CA19-9), prostate-specific antigen (PSA),[91] carcinoma antigen 125 (CA125),[92] colorectal cancer biomarker (CLD7),[93] and CA242,[94] are also crucial in this context. Analytical tests possessing sensitivity, specificity, reliability, and rapidity are pivotal in measuring these biomarkers and play a crucial role in the cancer detection process. The primary construction technique employed in MOF-based biosensors for analyzing cancer markers involves immobilizing biorecognition elements like antibodies, enzymes, or specific adapters to biomarkers such as antigens or specific targets. Various sensing techniques commonly combined with MOFs for biomarker detection include colorimetry, PEC, ECL, fluorescence, enzyme-linked immunosorbent assay (ELISA), radioimmunoassay (IRMA), surface-enhanced Raman spectroscopy, and mass spectrometry, as shown in Table 3.

For instance, Wei *et al.*[77] reported a surface-immobilized GO-based Zn-MOF biosensor using Zn^{2+} and TCPP, specifically for highly sensitive p53 antibody detection. Through the abundant loading of p53 antigens to recognize the target, they achieved an exceptional detection limit of 0.03 fg mL^{-1}. In another study,

Table 3 Recent progress in MOF-based carriers for disease treatment

No.	MOFs	MOF components	Cargo/drug	Stimuli type	Treatment goals	Main findings	References
1	Hollow porphyrinic MOF	Zr^{4+} and TCPP	Doxorubicin (DOX), indocyanine green (ICG)	pH, thermo	Carcinoma (4T1) cell	Release: 65% pH5 IC50: 0.11 μg mL^{-1} % Cell viability: 8%	22
2	PEG/PA@ZJU-64-NSN	Zn^{2+} and H_2BTDBA	Procainamide hydrochloride (PA)	pH	Heart, stomach (oral route)	Release: 100% (physiological environment), 40% (stomach environment)	176
3	Mg-MOF-74	Mg^{2+} and H_4dhtp	α-Cyano-4-hydroxycinnamate	—	HeLa	The saturated loading capacity: 625 mg g^{-1} % Cell viability: 5%	139
4	Curcumin@N_3-bio-MOF-100	Zn^{2+} and N_3-BPDC	Curcumin	pH	4T1	Release: 88.42% pH5	137
5	γ-Cyclodextrin-MOF@ Eudragit®RS	K^+ and γ-cyclodextrin	Indomethacin	—	Anti-inflammatory (oral route)	Release: 82.36%	160
6	MXene/MOF-5	Zn^{2+} and H_2BDC	Doxorubicin/pCRISPR	pH	HEK-293, PC12, HepG2, and HeLa	Release: 50% Loading efficiency (%): 46 % Cell viability: 9.9%	198
7	Fe_3O_4–NH_2@PDA@Au@MIL101-NH_2	Fe^{3+} and NH_2-BDC	Doxorubicin	Thermal	HeLa	The saturated loading capacity: 34.31 mg g^{-1} % Cell viability: 10%	124
8	Zn-MOF-74@CS	Zn^{2+}, Mn^{2+}, TEA, and H_4dhtp	Doxorubicin	—	HeLa	The saturated loading capacity: 113 mg g^{-} % Cell viability: 5%	125
9	HKUST-1	Cu^{2+} and trimesic acid	Paracetamol	—	Antipyretics and analgesics (oral route)	Loading efficiency (%): 63.41%	163
10	γ-Cyclodextrin-MOF	K^+ and γ-cyclodextrin	Florfenicol and enrofloxacin	—	Antibacterial (oral route)	MIC: +*E. coli*: 0.1 μg mL^{-1} +*S. aureus*: 1.6 μg mL^{-1}	168
11	Ru-90@bio-MOF-1	Zn^{2+} and BPDC	Ru-90	pH	Human melanoma A375, the non-tumor mouse L929	Release: 43.11% (pH 5), 25.36% (pH 7.4) IC50 (μM): 43.8 (A375), 31.5 (L929)	141
12	CS-g-PAA/PU/magnetic MIL-53	Fe^{3+} and terephthalic acid	Temozolomide and paclitaxel	pH, thermo	U-87 MG glioblastoma cells	Release: 90% at pH5, 43 °C % Cell viability: ∼25% Loading efficiency (%): 80	133
13	MgAl-LDH/Fe-MOF/D-Man	Al^{3+}, Mg^{2+}, and NH_2-BDC	Methotrexate, doxorubicin	pH	MDA-MB 231	Release: 45.2% (pH 5), 18.82% (pH 7.4)	122
14	Bio-MOF(Zn)@CMS/GQDs	Zn^{2+} and CMS/GQD	Curcumin, doxorubicin	pH	HepG2	Loading efficiency (%): CUR (54.2) and DOX (43.2)	199
15	FU@Eu-MOF	Eu^{3+} and H_3BTC	Fucoidan	pH	A549	Release: 85.3% pH 5	142
16	CuO-MOF	Fe^{3+} and $Cu_3(BTC)_2$	Doxorubicin	pH	—	Release: 98.9% pH 5	123
17	Bio-MOF/polydopamine	Zn^{2+} and curcumin	Doxorubicin	pH/NIR	HeLa	Release: 60.83% pH 5 IC50: 0.032 mg mL^{-1}	200
18	Zr MOF UiO-66	Zr^{4+} and BDC	Dichloroacetate, 5-fu	pH	MCF-7, HEK293	Loading efficiency (%): 27.5 IC50: 0.2 mg mL^{-1}	128
19	DOX/AS1411@PEGMA@GQDs@γ-CD-MOF	K^+ and γ-cyclodextrin	Doxorubicin	pH	MCF-7	Loading efficiency (%): 89.1%	201

Table 3 (*Contd.*)

No.	MOFs	MOF components	Cargo/drug	Stimuli type	Treatment goals	Main findings	References
20	CS/Zn-MOF@GO	Zn^{2+} and H_2BDC	5-Fu	pH	MCF-7	Loading efficiency (%): 45% Release: 41.47% pH 5	129
21	GQDs@Bio-MOF	Cd^{+} and TEA	5-Fu	pH	HT 29	Loading efficiency (%): 42.4% Release: 63.2% pH 5	202
22	Al-MOF/GO	Al^{3+} and GO	5-Fu	pH	MCF 7 and MCF 10A	Loading efficiency (%): 78.4% Release: 63.1%	130
23	DHA-UIO-66-NH_2	Zr^{4+} and BDC-NH_2	5-Fu	pH	MCF 7	IC50: 10.82 μM	203
24	UiO-66-NH_2	Zr^{4+}, BDC-NH_2	Temozolomide	Ultrasound intervention	U251, SHG44	Release: 100% % Cell viability: ~20%	134
25	ZnMOF-CS-FA	Zn^{2+} and TPA	Methotrexate	pH	HCT116	Loading efficiency (%): 78% Release: ~95% pH 5, ~25% pH 7.4	146
26	CMC/Cu-MOF	Cu^{2+} and terephthalic acid	Ibuprofen	pH	Anti-inflammatory (oral route)	Release: pH 1.2 (20%), pH 6.8 (40%), pH 7.4 (70%)	204
27	UiO-66-PDC	Zr^{4+} and H_2BDC	Ibuprofen	pH	Anti-inflammatory (oral route)	Release: pH 2 (10%), pH 7.4 (100%)	162
28	MIL-100/sodium dodecyl sulfate	Fe^{3+} and BTC	Insulin	pH	Diabetes treatment (oral route)	Release: 70% (pH 7.4)	172
29	ZIF-8	Zn^{2+} and 2-MIM	Indomethacin	pH	Anti-inflammatory (oral route)	Release: 90% The saturated loading capacity: 1210 mg g^{-1}	161
30	CMC-Zn-MEL@TC	Zn^{2+} and carboxymethyl cellulose	Tetracycline	pH	Antibacterial (oral route)	Release: 100% The antibacterial efficiency: +*E. coli*: 99% +*S. aureus*: 99%	170
31	Fe_3O_4@PAA@MIL-100(Cr)	—	Ciprofloxacin	pH	Antibacterial (oral route)	Loading efficiency: 50% Release: 80% at pH 7.4	205
32	ZIF-8/GO/$MgFe_2O_4$	Mg^{2+}, Zn^{2+}, and 2-methyl imidazole	Tetracycline	pH	Antibacterial (oral route)	Release: 92% at pH 7.4 Inhibition zone: +*E. coli*: 22 mm +*S. aureus*: 25 mm	169
33	U-CD-MOF	K^{+} and γ-cyclodextrin	Caffeic acid	pH	Antibacterial (oral route)	Release: 100%	171
34	UiO-67	Zr^{4+} and BDPC	Brimonidine	—	Eye drops	Adsorption capacity for the drug: 600 mg g^{-1} Release: 50%	177
35	SiRNA@MOF	Zn^{2+} and 2-methyl imidazole	TNFα siRNA	pH	Treatment of ulcerative colitis (oral route)	Release: +100% to 54.71% (pH 1.5), to 30.2% (pH 6.8) to 11.3% (pH 7.4)	206
36	NH_2-MIL101	—	Exendin-4	pH	Diabetes treatment (oral route)	Release: 100% pH 7.4	175
37	CD-MOF	K^{+} and γ-cyclodextrin	Honokiol	pH	Anticancer, control gastric acidity (oral)	Release: pH 1.2 (19%), pH 6.8 (46%), pH 7.4 (~94%)	173
38	MIL-100(Fe)	Fe^{3+} and H_3BTC	Genistein	pH	Antioxidant and antiangiogenic (oral route)	The saturated loading capacity: 271 mg g^{-1}	207
39	Bio-MOF-100	Zn^{2+} and 4,4′-biphenyldicarboxylic acid	Rifampicin, isoniazid, pyrazinamide	pH	Anti-tuberculosis (oral route)	Loading efficiency: 66% % Cell viability: 0%	208
40	MIL-100(Fe)	Fe^{2+} and BTC	Diclofenac	pH	Anti-osteoarthritis (oral route)	Release: 92% at pH 7.4	209

Hou *et al.*[86] evaluated the biosensing capabilities of N-doped porous carbon with active magnesium sites (Mg/NC-0.8) by annealing it with common coloring substrates like tetramethylbenzidine (TMB). They employed a Mg/NC-based colorimetric method to detect acetylcholinesterase (ACh), a cholinesterase associated with various neurodegenerative illnesses such as Parkinson's and Alzheimer's diseases. Abnormal ACh activity has been found linked to these illnesses. The principle underlying this sensing method involves the hydrolysis of acetylthiocholine (ATh) by ACh to produce thiocholine. Thiocholine, acting as a mercapto molecule, can reduce blue TMB back to its colorless form. The synthesized system ATh/Mg/NC-0.8/TMB successfully detected ACh with a low LOD of 0.0001 U L^{-1}. Addressing antigens, Hou *et al.*[95] devised a novel chemiluminescence sensing platform using Ag@ZIF-67 to detect carcinoembryonic antigens *via* base complementation between an aptamer and DNA strand. Their results showcased a wide linear detection range (0.0001–5 ng mL^{-1}) and a low detection limit of 0.00453 ng mL^{-1}. Recently, Ortega *et al.*[93] synthesized MIL-125-NH_2 coated with anti-CLD7 monoclonal antibody on a material using a microfluidic amperometric immunosensor device to detect the colorectal cancer biomarker. In this study, electrochemical immunosensors were used due to their rapidity, specificity, and feasibility.[96] In addition, this technique relies on the specific affinity between antibodies and antigens to quantify early disease detection. Specifically, the electrochemical change caused by antigen–antibody hybridization is converted into a measurable signal. To perform this technique, the MOF material acts as a bridge connecting many anti-CD7 antibodies to the central channel surface. The central channel was then thoroughly washed to remove unbound antibodies, while bound antibodies remained stably immobilized for at least 1 month. It is those antibodies that bind to the corresponding antigens in diseased cells, causing an electrical signal if any. Accordingly, they achieved a LOD value of 0.1 pg mL^{-1} in the range from 2 to 1000 pg mL^{-1}.

3.3. MicroRNAs

MicroRNAs (miRNAs) are small non-protein-coding RNAs that modulate post-transcriptional gene expression by targeting

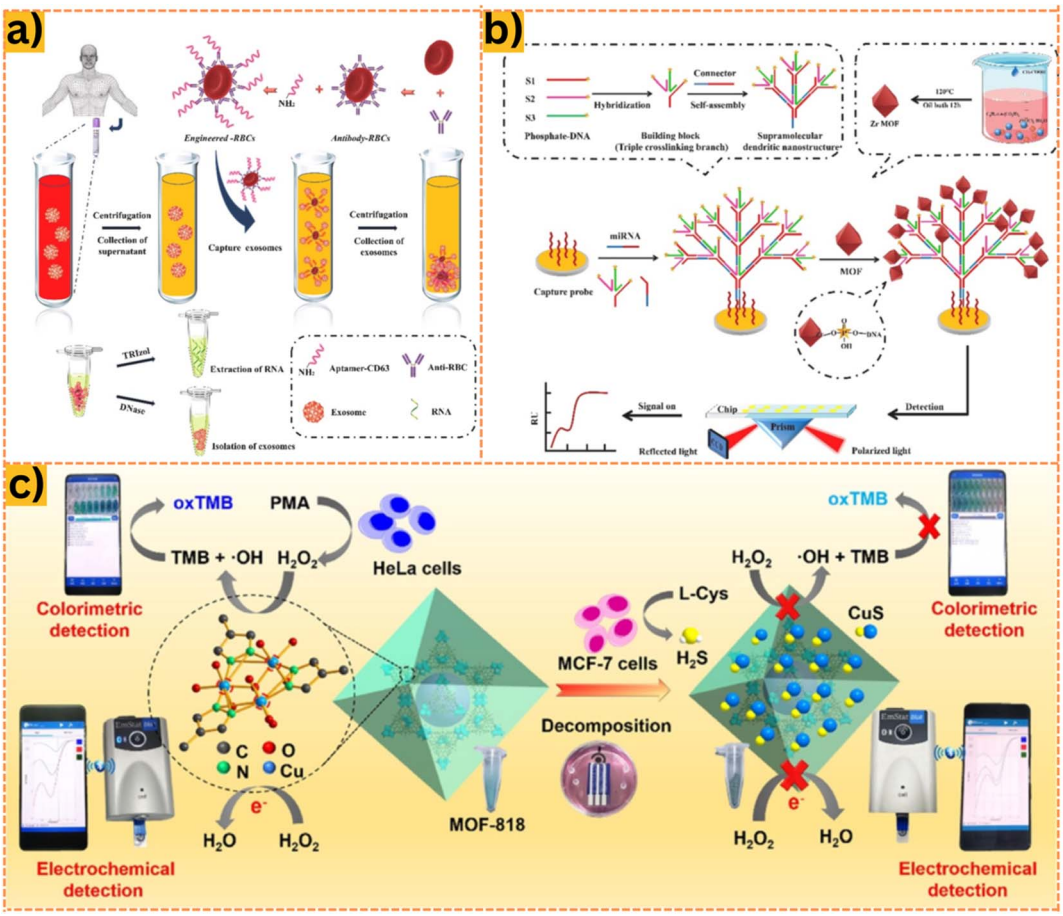

Fig. 3 (a) Principle of action of ICDSE for exosome enrichment from NSCLC patient plasma: Synthesis of engineered erythrocytes to obtain exosomes or exosomal cargo using CD63 aptamer biological affinity. (b) Exosomal miRNA installation based on the fabrication of a plasmonic biosensor based on supramolecular dendritic nanostructures and Zr MOF. Reproduced from ref. 103 with permission from Elsevier, copyright 2023. (c) Colorimetric and electrochemical sensing method based on MOF-818 on a smartphone platform, developing a H_2O_2 sensing system from living cells. Reproduced from ref. 104 with permission from Elsevier, copyright 2022.

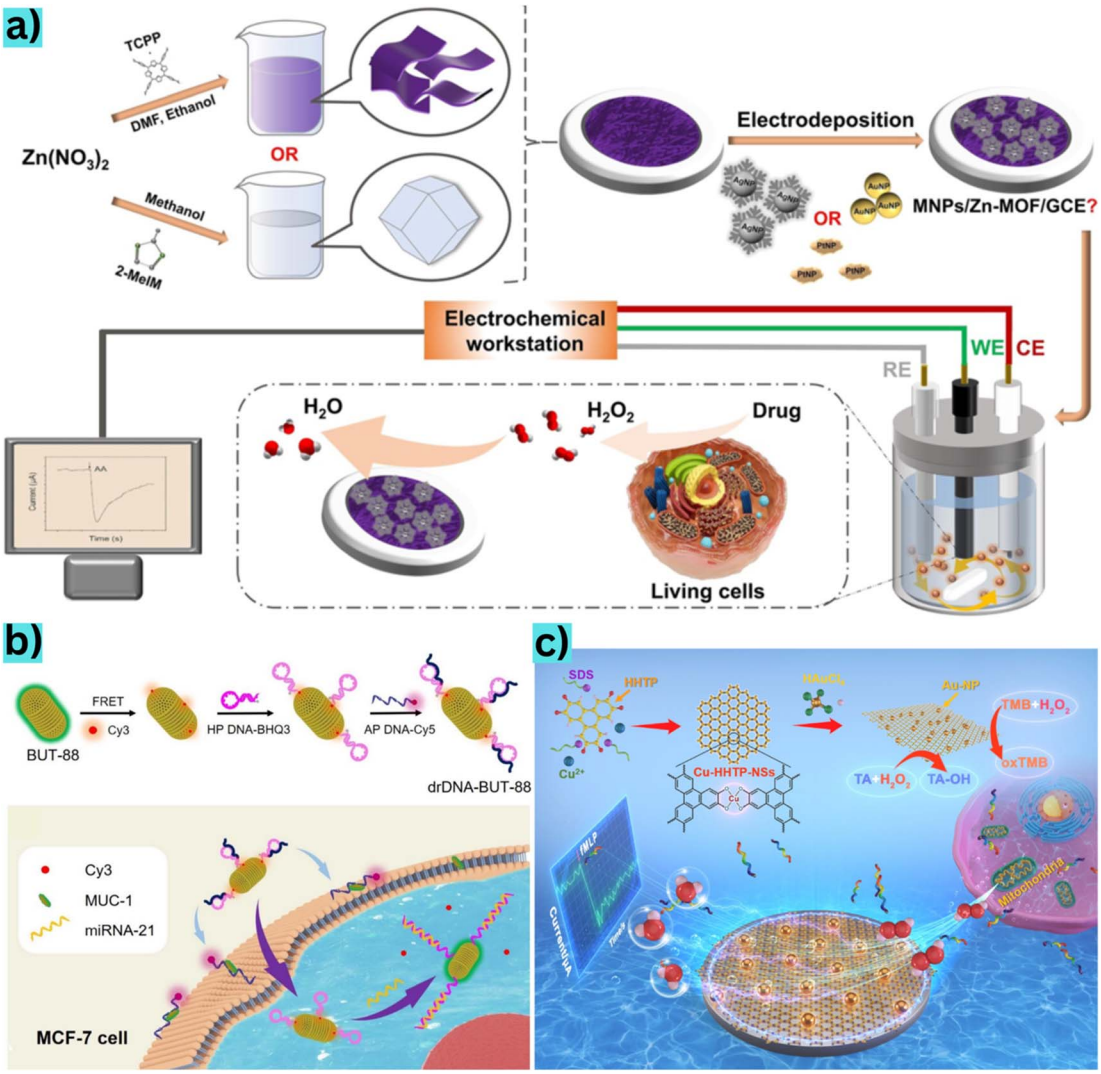

Fig. 4 (a) Manufacturing process of the MNPs/Zn-MOF modified electrode and H_2O_2 sensor from living cells released from drug stimulation and data transmission to the electrochemical station. Reproduced from ref. 112 with permission from American Chemical Society, copyright 2022. (b) BUT-88-based DNA probe fabrication procedure for cytoplasmic miRNA-21 diagnosis in MCF-7 cells and simultaneous membrane-specific recognition of MUC-1. Reproduced from ref. 28 with permission from Wiley-VCH Verlag, copyright 2020. (c) Schematic description of materials synthesis and use of Au@Cu-HHTP-NS modified electrodes to sense H_2O_2 in mitochondria from living human colon cells. Reproduced from ref. 84 with permission from Elsevier, copyright 2022.

specific mRNA molecules.[97] Recent studies have revealed that miRNAs circulate in a cell-free, remarkably stable form, detectable in plasma and serum within the bloodstream.[98] Moreover, tumor cells demonstrate the ability to release miRNAs into circulation. Alterations in plasma and serum miRNA profiles have been observed in various disease states, including cancer.[99] Detection of miRNAs typically relies on the hybridization of probe DNA sequences with the miRNA analyte.[100] Single DNA strands can be securely immobilized on MOFs and MOF-based composites through interactions like π-stacking, electrostatics, and hydrogen bonding.[101]

Kong *et al.*[28] developed a MOF-based biosensor using Zr^{4+} and TCTA, decorated with HP DNA, capable of precisely identifying miRNA-21 within the cytoplasm. This biosensor exhibited a limit of detection (LOD) of 0.13 nM within the range of 0.2–1.0 nM. In another study, Jiang *et al.*[102] synthesized the Co-MOF material based on an electrochemiluminescence biosensor platform (ECL) carrying *N*-(4-aminobutyl)-*N*-ethylisoluminol (ABEI) to enhance efficiency. The Co-MOF, characterized by high porosity, facilitated the covalent binding of probe DNA for easy detection of miRNA-21, termed Co-MOF-ABEI/$Ti_3C_2T_x$. This designed ECL MOF-based biosensor successfully identified miRNA-21 extracted from HeLa cells, achieving an impressive detection limit of 3.7 fM. Recently, Fan *et al.*[103] introduced an innovative integrated concentration and determination system of exosomes (ICDSE) to enrich plasma exosomes from non-small cell lung cancer patients. This system efficiently extracted miRNA-15 without the need for expensive equipment or reagents, providing a cost-effective solution for detection applications. For miRNA detection, four types of DNA with specific complementary sequences

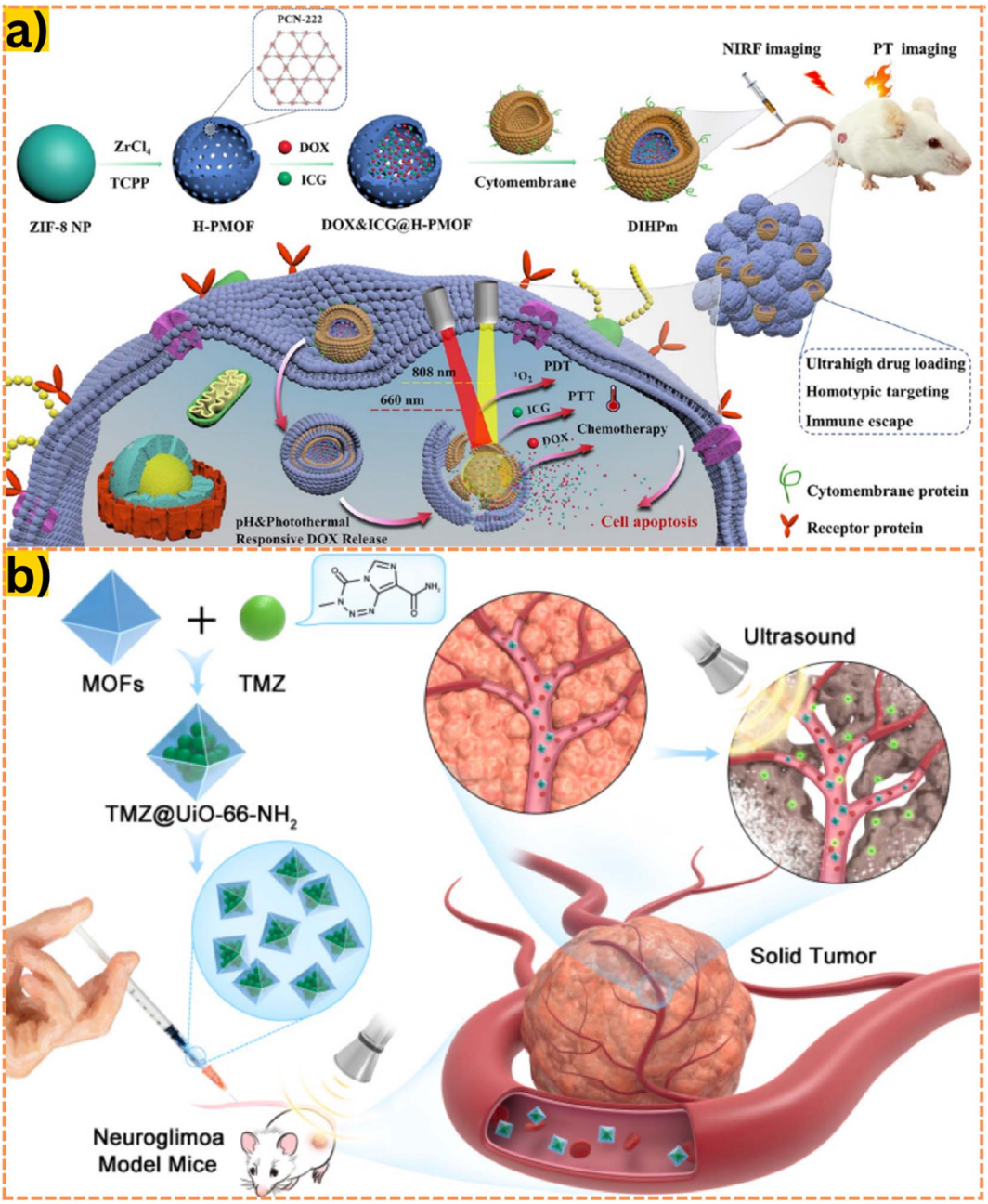

Fig. 5 (a) During the synthesis process, a hollow porphyrinic ZIF-8-based composite is co-loaded with DOX and ICG and coated with cytomembrane for homotypic targeting and immune escape. As this material enters the bloodstream to the cancer cells under a pH response, they release ICGs and DOXs for PDT, PTT, and chemotherapy. Alternatively, the carrier can be irradiated with NIR to generate drugs and $^1O_2$, which induce PDT effects and kills cancer cells. Reproduced from ref. 22 with permission from American Chemical Society, copyright 2021. (b) A temozolomide drug delivery system based on MOF is injected directly into the mouse; the drug is transported through the bloodstream into nerve cells under the influence of ultrasound waves. Through this approach, the carrier easily penetrates the blood–brain barrier (BBB) and completely releases the drugs. Reproduced from ref. 134 with permission from Dove Medical Press Ltd, copyright 2021.

were injected into Zr-MOF on an SPRi chip to identify miRNA-155, as depicted in Fig. 3. Leveraging the significantly high refractive index of zirconium metal–organic framework, the biosensor achieved an impressive LOD for miRNA-155, not exceeding 2.03 fM. Furthermore, this study pioneered the engineering of erythrocytes by functionalizing natural human erythrocytes with aptamers on MOFs, demonstrating promising advancements in this field.

3.4. Living cancer cells

Cancer is a disease characterized by the rapid proliferation of malignant cells, posing a significant threat to human health.[105] Detecting cancer cells early can substantially improve the chances of timely intervention and increase survival rates.[106] These cells are recognized by their increased production of glycans and proteins.[107] Consequently, probes specifically

designed to bind to these glycans or proteins within cancer cells offer a feasible approach for cancer diagnosis.[75] Therefore, understanding the immobilization and stability of the carrier material for these probes is crucial in identifying cancer cells. MOFs present an attractive option as carriers for binding biomolecules such as antibodies, DNA, or aptamers onto sensors for detecting various targets.[108–110] Their high surface area, well-defined organic ligands, and adjustable porosity make them suitable candidates. By optimizing synthesis conditions and modifying the chemical properties of MOFs, they can potentially exhibit electrochemical activity and an efficient binding capacity, serving as carriers for detecting living cancer cells.

Duan *et al.*[78] designed an electrochemical Cr-MOF-based biosensor loaded with CoPc nanoparticles to detect the colorectal carcinoma cell line (CT26). Their results demonstrated a linear detection range for CT26 cells from 50 to 1.0×10^7 cells mL^{-1}, with a low LOD of 31 cells mL^{-1}. The authors highlighted the microporous structure and large specific surface area of the MOF material, enabling substantial anchoring of cobalt phthalocyanine (CoPc) nanoparticles within the pore channels of Cr-MOF. This integration enhanced the interaction and fixation of aptamer DNA, stabilizing the formed aptamer–cell complex. Consequently, MOF@CoPc exhibited robust electrochemical activity and high sensitivity in detecting cancer cells. In the same trend, Li *et al.*[111] synthesized Zr-MOF (UiO-66-2NH_2) to develop an aptasensor with high electrochemical efficiency for detecting breast cancer cells. They utilized their own material ligand (2,5-diaminoterephthalic acid) as a platform to immobilize the aptamer, binding it to the PO4-aptamer through electrostatic interactions, stacking, and covalent bonds. Consistent with the study of Duan *et al.*,[78] the limit of detection was found to be 31 cells mL^{-1}. This underscores the capacity of MOFs to anchor aptamers without requiring an intermediate material for capture. Furthermore, the outstanding biocompatibility of the MOF carrier facilitated the long-term immobilization of aptamer chains and the identification of living cancer cells (Fig. 4).

4. MOF-based carriers in drug delivery systems

4.1. Blood cell-based drug delivery

The limited selectivity and adverse effects of conventional chemotherapy have led to the development of material-based drug delivery systems.[113] Hence, there is a need to create a controlled blood delivery system to mitigate these drawbacks and enhance the therapeutic effectiveness of drugs.[114] This approach aims to improve the anti-cancer impact of drugs with precision, targeting specific areas, and ensuring efficacy. In recent years, MOFs, composed of metal ion clusters connected by organic bonds in a porous structure, have gained significant attention.[115] They have emerged as a prominent technology in blood drug delivery research due to their unique physical structures and versatile applications. MOFs possess exceptional properties including adaptable composition and structure, customizable dimensions, flexible functionalities, high drug payload capacity, and high biocompatibility. These attributes position them as promising candidates for delivering drugs through the bloodstream.[116] MOFs are capable of selectively transporting drugs between normal cells and tumor cells within the bloodstream, exploiting variations in conditions such as pH and temperature between these cell types.[117] Beyond drug delivery, MOFs can also serve as Fenton reaction agents, catalyzing the conversion of H_2O_2 to O_2 while producing $^{\bullet}OH$ to target and eliminate more cancer cells.[118] Therefore, the evolution of MOF-based drug carrier design technology represents a new frontier in biomedical research, offering a wide array of possibilities for cancer treatment.

Doxorubicin (DOX) is a widely used chemotherapeutic medication for treating various malignancies such as bladder cancer, breast cancer, and acute lymphocytic leukemia.[119] MOFs have shown potential in tumor synergistic therapy by effectively loading DOX through hydrogen bonding or electrostatic interactions and subsequently releasing it (Fig. 5a).[120] MOFs also exhibit pH-responsive drug release properties, with DOX being primarily released at acidic pH levels (pH 5 and pH 2) rather than at pH 7.4. This behavior is attributed to the degradation of MOFs under acidic conditions, making them suitable for releasing drugs in low pH environments.[121] Indeed, Pooresmaeil and Namazi[122] demonstrated that drug release from MgAl-LDH/Fe-MOF/D-Man was significantly higher at pH 5.0 (45.2%) compared to that at pH 7.4 (18.82%). More highly, Gharehdaghi *et al.*[123] observed that the MOF-based carrier CuO-MOF released 98.9% of DOX at pH 5, whereas only 33.5% was released at pH 7.4. Further investigations by Li *et al.*[124] explored the saturated loading capacity of DOX in MOFs using Fe_3O_4–NH_2@-PDA@Au@MIL101-NH_2, reaching a maximum loading capacity of 34.31 mg g^{-1}. Hu *et al.*[125] reported an even higher saturated loading capacity of Zn-MOF-74@CS (113 mg g^{-1}), which was 3.3 times greater than that in the work done by Li *et al.*[124] These findings collectively demonstrate the potential of MOFs as a promising choice for drug delivery in cancer therapy due to their pH-responsive drug release mechanisms and high drug loading capacities.

5-Fluorouracil (5-FU), initially introduced as a synthetic antineoplastic agent decades ago, remains a prominent treatment for various common malignancies, including colorectal and breast cancer.[126] Its mechanism involves the irreversible inhibition of thymidylate synthase, disrupting the synthesis of DNA and RNA in cancer cells. Classified as an anti-metabolite, 5-FU exerts its action by interfering with cell nucleotide metabolism.[127] For instance, Abánades Lázaro *et al.*[128] introduced a MOF-based carrier, Zr MOF UiO-66 (formed using Zr^{4+} and BDC), to combat MCF-7 cancer cells. Their work revealed an IC50 value of 0.2 mg mL^{-1} with a MOF loading efficiency of 27.5%. In comparison, Pooresmaeil *et al.*[129] developed CS/Zn-MOF@GO, comprising Zn-MOF doped graphene oxide (GO) and chitosan (CS), exhibiting a higher loading capacity of 45%. This increase was attributed to the supportive high porosity of GO within the MOFs, enhancing drug loading. Additionally, CS imparted sensitivity to low pH, resulting in a drug release activity of 41.47% at pH 5. Similarly, Aghazadeh Asl *et al.*[130] synthesized CS/Al-MOF/GO, integrating Al-MOFs with GO

nanosheets coated with pH-sensitive CS for 5-FU delivery against MCF-7 cells. Their study significantly improved drug loading efficiency, achieving up to 78.4%. Notably, the release activity of 5-FU from the MOF reached 63.15% at pH 5. These studies underscore the potential of MOFs as effective carriers for 5-FU delivery in cancer treatment.

Temozolomide (TMZ) is an alkylating chemotherapy agent primarily used to treat certain brain cancers. It is also considered a second-line treatment for astrocytoma and is presently the sole first-line chemotherapy for malignant glioma.[131] However, due to its limited water solubility and potential toxicity, TMZ is deemed ineffective and harmful to normal cells.[132] In an intriguing study, Bazzazzadeh *et al.*[133] proposed a drug delivery system, CS-g-PAA/PU supported by a MOF termed CS-g-PAA/PU/MIL-53, loaded with TMZ for U-87 treatment. The investigation focused on the drug release activity under varying conditions of pH (7.4 and 5.5) and temperature (37 and 43 °C), yielding optimal release (90%) at pH 5 and 43 °C. The decreased pH led to increased swelling of materials due to the ionization of amino and carboxylic groups within CS-g-PAA, while higher temperature possibly influenced the opening of MOF pores, optimizing drug release efficiency. This advancement holds potential for future therapies combining hyperthermia and chemotherapy. More effectively, Wan *et al.*[134] synthesized the UiO-66-NH_2 material to deliver TMZ to penetrate the blood–brain barrier using ultrasound intervention. High-intensity ultrasound waves can temporarily disrupt the BBB without damaging surrounding nerve tissue as shown in Fig. 5b.[135,136] Indeed, the drug release activity achieved 100% after only 25 minutes under ultrasound. This efficient release could be attributed to the ultrasound-assisted enhancement of TMZ solubility in the bloodstream and the slow-release nature of UiO-66-NH_2.

Besides the previously mentioned drugs, various others have been explored in building MOF-based drug delivery systems. Alves *et al.*[137] synthesized curcumin@N_3-bio-MOF-100, composed of Zn^{2+} and N_3-BPDC, for curcumin delivery to 41T cells. Curcumin, a natural compound extracted from *Curcuma longa*, has demonstrated effectiveness against several cancers, including breast cancer.[138] The curcumin release rate of MOF was 88.42% at pH 5. In another study, Hu *et al.*[139] utilized α-cyano-4-hydroxycinnamate, an intracellular lactate transport inhibitor,[140] loaded into Mg-MOF-74. These materials exhibited excellent drug loading potential, achieving a high saturated loading capacity of 625 mg g^{-1}. The percentage of cell viability for HeLa cells was notably low at only 5%. Marson Armando *et al.*[141] synthesized Bio-MOF-1, a porous microcrystalline material demonstrating significant loading capacity for the anticancer metallurgical drug Ru-90, effective against A375 and L929 cells. The Zn-MOF showed a drug release capacity of 43% and 25% at pH 7.4 and pH 5.0, respectively. Moreover, Raju *et al.*[142] designed a pH-responsive Eu-MOF decorated with Fucoidan, a sulphated polysaccharide found in brown seaweeds with anti-tumor activities.[143] The drug release from Eu-MOF exhibited 85.3% effectiveness against A549 cells. In addition to the above drugs, methotrexate (MTX), a folic acid analog widely used against various cancers,[144,145] was loaded onto Zn-MOF coated with folic acid-chitosan (ZnMOF-CS-FA) by Khatibi *et al.*[146] The study demonstrated that the release of MTX by the MOF was up to 10 times higher at low pH (pH 5) compared to neutral pH (pH 7.4). These findings suggest that leveraging MOFs in drug delivery can address drawbacks such as poor solubility and targeting ability in drug molecules, potentially improving their efficacy in the bloodstream.

4.2. Oral drug delivery

Oral drug delivery has long been a preferred method due to its safety, high compliance, and cost-effectiveness.[147] However, challenges persist due to poor gastrointestinal stability and presystemic metabolism, necessitating support systems for effective delivery.[148] Typically, drugs are absorbed in the small intestine, heavily perfused and a site for metabolism. Yet, these drugs face digestion under the harsh acidic conditions of the stomach, leading to solubility issues and reduced bioavailability.[149,150] To overcome these challenges, oral drug transporters are under development. These aim to aid drug penetration through the mucus barrier and shield the loaded drug from damage caused by gastric acids. MOFs have shown promise in drug delivery, but their susceptibility to destruction in stomach acidity limits their use. Bunzen[151] indicated that MOF decomposition is primarily due to the competition between protons and metal ions for coordination with organic ligands. MOF stability in acidic environments hinges on the composition, where materials with high-valence metal ions and carboxylate ligands demonstrate greater stability. Conversely, those based on low-valent metal ions and azolate ligands exhibit high instability under acidic conditions.[152] Consequently, selecting MOFs aligned with the pH environment or modifying MOFs post-synthesis appears as a viable strategy for effective oral drug administration.

The proposed mechanism for utilizing MOFs as an oral drug delivery agent involves employing MOFs as drug carriers alongside pH-sensitive materials for coating (Fig. 6). This composite acts as a gate switch, preventing unexpected drug leakage and enhancing the biocompatibility of the delivery system.[153] The drug is loaded onto either the MOF material or MOF-based modified material and encapsulated within a capsule. Upon ingestion, the drug-material moves through the esophagus into the stomach, where it can decompose in the acidic environment.[154] Thanks to the protective nature of MOFs, the drug is released gradually in small amounts.[74] As the composite moves into the basic environment of the small intestine, the MOF, having been modified accordingly, opens its pores and releases the drug. The mechanism of proton-induced coordination disruption is commonly employed to achieve pH-based drug release.[155] Once released, the drug is absorbed into the intestinal mucosa and enters the bloodstream for distribution to target organs.[156] Presently, studies have not been directly conducted on humans; instead, simulations are performed to mimic conditions in each environment. Laboratory simulations involve subjecting the material to three pH landmarks corresponding to gastric juice, and the initial and secondary regions of intestinal juice. Initially soaked at pH 1.2,

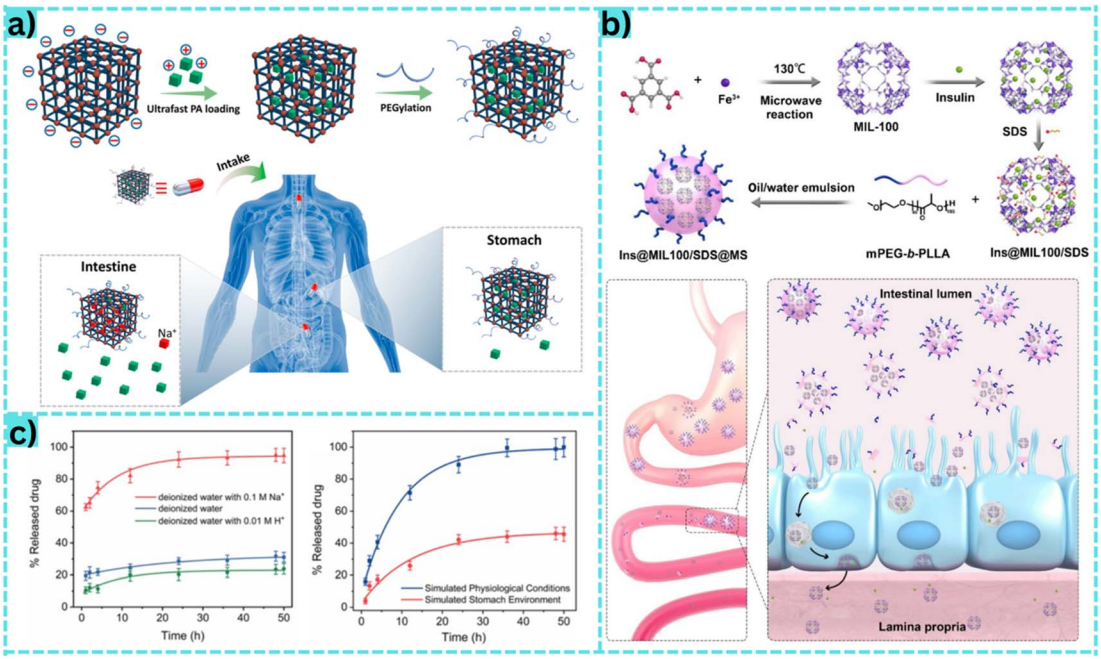

Fig. 6 (a) The mechanism of the MOF material for oral drug delivery, the drug passes through the stomach and is absorbed in the intestine. Reproduced from ref. 176 with permission from Elsevier, copyright 2022. (b) The synthesis and functionalization of MOFs facilitate their absorption into the small intestinal cell wall, where they gradually undergo breakdown as they traverse each layer. Initially, they navigate through the upper tissue layer by shedding the PEG layer. Subsequently, they enter the lamina propria, a region supporting epithelial cells and facilitating the passage of blood vessels and nutrients. At this stage, the MOF material releases insulin drugs, which enter the bloodstream to perform their intended function. Reproduced from ref. 172 with permission from American Chemical Society, copyright 2020. (c) The graph (left) shows the drug release mechanism from MOF materials in three types of media: deionized water, deionized water with 0.01 M H^+ and deionized water with 0.01 M Na^+. Accordingly, drug release was highest in deionized water with 0.01 M Na^+, thus indicating that H^+ could not trigger procainamide release from PEG@ZJU-64-NSN. This indicated that there was a strong interaction between the cationic procainamide and the anionic MOF framework. This strong interaction would be further enhanced by procainamide protonation under more acidic conditions. The graph (right) shows the drug release ability of the material in two simulated environments: the physiological environment and the acidic environment of the stomach. Reproduced from ref. 176 with permission from Elsevier, copyright 2022.

the material is then transferred at defined intervals to buffer solutions of pH 6.8 and pH 7.4. Additionally, gastric acid solution and pepsin are used to replicate the environment in the body and test the oral drug delivery capability of MOFs.[157]

4.2.1 Antipyretics and analgesics. Fevers significantly disrupt daily life and pose potential risks for various illnesses. They typically accompany mild to severe illnesses affecting a significant portion of the global population. Beyond elevated body temperature, fevers bring forth a range of manifestations, including physiological changes and immune as well as metabolic reactions in the body. Several drugs, such as indomethacin, paracetamol, ibuprofen, and aspirin, are extensively used to manage pain, fever, and inflammation.[158] However, their limited bioavailability results in incomplete treatment, prompting patients to increase dosages and leading to heightened drug resistance. These drugs, due to their poor water solubility, often require additional excipients from pharmaceutical companies to enhance their oral availability. The use of MOFs as drug carriers has gained widespread traction to augment drug effectiveness at specific absorption sites and improve solubility. The initial report on employing MOFs by Horcajada *et al.*[159] for ibuprofen drug delivery in 2006, focusing on MIL-100 and MIL-101, marked the beginning of an era in drug delivery using MOF materials. This research heralded a new phase in biomedical technology aimed at supporting disease treatment.

For instance, Wang *et al.*[160] developed the MOF-based oral indomethacin delivery system, IMC/CD-MOF@ERS, comprising γ-cyclodextrin and K^+ encapsulated with the polymer Eudragit®RS. With the MOF support, this system achieved an 82.36% drug release activity. In comparison, Ohsaki *et al.*[161] demonstrated ZIF-8 as a carrier for indomethacin, achieving over 90% drug release, surpassing the study by Wang *et al.*[160] ZIF-8 notably exhibited significantly improved bioavailability of indomethacin, not only through pH-sensitive response but also by enhancing the water solubility of the drug. In another instance, Wang *et al.*[162] synthesized UiO-66, composed of Zr^{4+} and H_2BDC ligands, as a targeted release platform for the oral anti-inflammatory drug ibuprofen. The release behaviors of IBU@UiO-66 showed 10% release at pH 2 and 100% release at pH 7.4. Moreover, Gautam *et al.*[163] synthesized HKUST-1, comprising Cu^{2+} and trimesic acid through a hydrothermal route, for transporting paracetamol. Their findings revealed a MOF loading efficiency of 63.41%.

4.2.2 Antibacterial. Premature release of antibiotics along their path can induce numerous side effects that impact human health.[164] For instance, tetracycline, widely used in treating diseases like malaria, plague, and brucellosis, is known to irritate the gastrointestinal tract, causing discomfort and health issues.[165,166] Early dissolution of antibiotics in the stomach can result in nausea, stomach pain, epigastric discomfort, and even stomach ulcers.[167] Thus, an engineered drug delivery system is necessary to ensure biocompatibility in the dosage form, enabling dissolution in the intestines while mitigating gastrointestinal irritation and related side effects. Materials exhibiting substantial surface areas and high pore volumes, such as MOFs, emerge as promising candidates for designing drug delivery systems that enhance effectiveness and minimize adverse drug effects.

Recently, Wei *et al.*[168] synthesized γ-cyclodextrin-MOF from K^+ and γ-cyclodextrin to deliver florfenicol and enrofloxacin synergistically, targeting *E. coli* and *S. aureus*. Accordingly, MIC values obtained were 0.1 μg mL^{-1} for *E. coli* and 1.6 μg mL^{-1} for *S. aureus*. In another study, Sanaei-Rad *et al.*[169] fabricated ZIF-8/GO/$MgFe_2O_4$ consisting of Mg^{2+}, Zn^{2+} and 2-methyl imidazole for tetracycline transport. The achieved results showed that 92% tetracycline was released at pH 7.4. Similarly, Alsaaed *et al.*[170] utilized carboxymethyl cellulose as ligands to synthesize CMC-Zn-MEL, which was adorned with tetracycline. This formulation exhibited a higher drug release efficiency (100%) compared to that of Sanaei-Rad *et al.*[169] Interestingly, an antibacterial efficacy of 99% was achieved against both *E. coli* and *S. aureus*. In line with this trend, Shen *et al.*[171] reported the synthesis of U-CD-MOF composed of K^+ and γ-cyclodextrin for carrying caffeic acid. Experimental findings indicated a 100% release of caffeic acid at pH 7.4.

4.2.3 Other diseases. Aside from their common oral drug applications, MOFs are utilized in delivering drugs for a wide array of diseases. For example, Zhou *et al.*[172] synthesized MIL-100(Fe) using Fe^{3+} and BTC ligands, coating it with sodium dodecyl sulfate as a pH-sensitive component for insulin delivery. Their experiments showed the highest drug release (70%) at pH 7.4. In another study, He *et al.*[173] used K^+ and γ-cyclodextrin to fabricate CD-MOF for transporting honokiol, a compound indicated for neuroprotective, antispasmodic, antidepressant, anti-tumor, and anti-cancer treatments.[174] Notably, they activated CD@MOF using supercritical carbon dioxide ($scCO_2$) technology for the first time. This technique enhanced the surface area and pore volume without clogging channels or collapsing the framework. The surface area of activated CD@MOF reached 1902.9 m^2 g^{-1}, doube that of the non-activated material (1140.3 m^2 g^{-1}). Additionally, the high diffusivity of $scCO_2$ enabled substantial drug molecule delivery into CD@MOF pores, suggesting a promising biomedical application technology. The results showed the activated material doubled the drug loading capacity compared to the control. In another instance, Zhou *et al.*[175] successfully synthesized NH_2-MIL101 to carry exendin-4 for diabetes treatment, achieving 100% drug release at pH 7.4. Jiang *et al.*[176] produced PEG/PA@ZJU-64-NSN to load procainamide hydrochloride for antiarrhythmic purposes, showing 100% and 40% drug release in physiological and stomach environments respectively (Fig. 6c). These research demonstrations of MOF materials in drug delivery signify substantial contributions to future biomedical technology and materials science.

4.3. Other drug delivery routes

Besides drug delivery through the blood and oral routes, MOFs can be agents that carry drugs through other routes such as dermal and ocular administration. For ocular drug delivery, MOFs are applied in this field as a new step to overcome the challenges of conventional eye drops. In the past, eye drops often suffered from low bioavailability due to tear turnover, rapid nasal drainage, and reflex blinking. Therefore, many manufacturers increase the dosage of the drug in the solution. This increase leads to many consequences related to toxicity and unwanted side effects. From the above motivations, Gandara-Loe *et al.*[177] demonstrated the potential applicability of MOFs in eye drops. Their work with UiO-67 showcased an adsorption capacity of 600 mg g^{-1} for the brimonidine eye drug. In addition, the drug release percentage was achieved up to 50% after 12 days. Regarding transdermal delivery, there are very few studies presenting in-depth the features of MOFs in transdermal drug delivery. The driving force behind transdermal drug delivery is the negative effects of oral drugs on the stomach. Furthermore, injecting drugs is complicated because it is difficult to perform on your own and requires the assistance of specialized staff. Therefore, the transdermal drug delivery route is considered a simple and non-invasive way that is convenient even for self-administration. Indeed, Rojas *et al.*[178] synthesized three types of MOFs, UiO-66, MIL-100 and MIL-127, to deliver two drugs ibuprofen and aspirin through the skin. The results obtained indicated that UiO-66 had the highest drug loading content of 92%, while MIL-100 demonstrated excellent drug release up to 99% after 1 day under simulated skin conditions. However, the desirable properties of MOFs for topical treatments differ significantly from those required for other routes of administration. Therefore, they require an in-depth understanding of the drug delivery route, stability and drug delivery time of MOFs.

5. Limitations and future prospects

MOFs are strategically designed to optimize their properties for biomedical applications, including direct injection or oral ingestion for tasks like sensing substances, aiding imaging, and treating diseases. However, the complex nature of the human body necessitates a thorough comprehension of materials introduced directly into it. Presently, comprehensive mechanisms outlining the fate of MOFs in various applications remain incomplete. Specifically, the utilization of MOF materials in resonance imaging or biomarker sensing within living organisms lacks specific elucidation. Moreover, the mechanisms for blood–brain barrier drug delivery using MOFs for neurological disease treatment are nascent. Similarly, precise pharmacokinetic routes, especially for oral drug delivery, remain

undetermined, with most studies only simulating physiological environments. Consequently, uncertainties persist regarding whether MOFs can manifest their full potential within the human body as observed in laboratory settings. Predictions regarding the long-term toxicity of MOFs when interacting with organs remain elusive, despite some studies on biocompatibility. Additionally, assessments of MOF stability under real stomach conditions, characterized by varying acid types and potential interactions with food ingredients, are lacking. Moreover, the pathways of MOF elimination post-treatment and their potential impact on the excretory system in the body are unclear. These gaps underscore the need for further research and comprehensive exploration of MOFs in biomedical technology to address these limitations.

Despite their current limitations, MOFs indeed hold immense promise for future biomedical and technological advancements. Their unique characteristics, such as large surface areas and pore volumes, render them ideal for pollutant collection in water treatment.[179] Research into the removal of various pollutants – ranging from heavy metal ions to organic dyes – leveraging different MOF properties has showcased their remarkable potential in this domain.[180] Their stability in water, high surface area, efficient adsorption, and compositional adaptability make them valuable assets in environmental studies.[181] Furthermore, in the pursuit of clean energy storage and distribution, MOFs have emerged as crucial components.[182] They play pivotal roles in energy storage and conversion, contributing to advancements in battery technologies like lithium–sulfur, lithium–oxygen, and zinc–air batteries, as well as supercapacitors.[183] Additionally, their unique nature as inorganic-organic hybrid materials marks a breakthrough in gas separation membranes. The production of highly porous MOFs for gas separation has gained traction, enabling the molecular-scale separation of gases through methods like C_3H_6 purification, C_2H_4 purification, noble gas separation, and isotope separation.[184,185] We anticipate that the MOF materials will provide important potential for future research into multifunctional system fabrication. They can expand the industrial scale and bring outstanding features to human life.

6. Conclusion

Thanks to their exceptional functionality and versatility, MOF-based nanomaterials exhibited remarkable progress in various biomedical applications. MOF-based biosensors with a high degree of porosity, stability, uniformity, and biocompatibility are promising in sensing H_2O_2, tumor biomarkers, microRNA, and detecting living cancer cells. Moreover, well-designed MOF-based carriers have proven effective in drug delivery systems and anticancer therapies, leveraging their superior properties. However, certain aspects, such as new surface modification strategies and pre-clinical trials of MOF-based materials, should require critical consideration. Challenges in understanding the release of metallic ions, dopants, or ligands during interactions with enzymes, proteins, normal cells, and cancer cells are still existing. Additionally, concerns regarding potential toxicity, bioaccumulation, and long-term effects remain largely unexplored. Despite these inherent shortcomings and areas needing further investigation, MOFs hold immense promise for future biomedical therapeutic applications and continue to demonstrate outstanding functionalities across various fields.

Conflicts of interest

There are no conflicts to declare.

Acknowledgements

We acknowledge Ho Chi Minh City University of Technology (HCMUT) and VNU-HCM for supporting this study.

References

1 K. Shimizu, S. Hibino, M. H. Biros, T. Irisawa and T. Shimazu, *Int. J. Emerg. Med.*, 2021, **14**, 2.
2 L. L. Tundisi, J. A. Ataide, J. S. R. Costa, D. de F. Coêlho, R. B. Liszbinski, A. M. Lopes, L. Oliveira-Nascimento, M. B. de Jesus, A. F. Jozala, C. Ehrhardt and P. G. Mazzola, *Colloids Surf., B*, 2023, **222**, 113043.
3 S. Liu, J. Tang, F. Ji, W. Lin and S. Chen, *Gels*, 2022, **8**, 46.
4 B. Rabeie and N. M. Mahmoodi, *J. Colloid Interface Sci.*, 2024, **654**, 495–522.
5 N. Ahmad, N. A. H. M. Nordin, J. Jaafar, A. F. Ismail and M. K. N. B. Ramli, *J. Environ. Chem. Eng.*, 2021, **9**, 105887.
6 H. Hoseinzadeh, M. Bakhtiari, K. Seifpanahi-Shabani, M. Oveisi, B. Hayati, B. Rabeie, F. Shahmoradi Ghaheh, R. Salmani and H. Ullah, *Mater. Sci. Eng., B*, 2021, **274**, 115495.
7 Y. Mantri and J. V. Jokerst, *ACS Nano*, 2020, **14**, 9408–9422.
8 L. Chen, W. Hong, W. Ren, T. Xu, Z. Qian and Z. He, *Signal Transduction Targeted Ther.*, 2021, **6**, 225.
9 Z. Edis, J. Wang, M. K. Waqas, M. Ijaz and M. Ijaz, *Int. J. Nanomed.*, 2021, **16**, 1313–1330.
10 M. Alavi, *Expert Rev. Anti-Infect. Ther.*, 2022, **20**, 897–906.
11 E. N. Hammad, S. S. Salem, A. A. Mohamed and W. El-Dougdoug, *Appl. Biochem. Biotechnol.*, 2022, **194**, 6053–6067.
12 S. S. Salem, M. S. E. M. Badawy, A. A. Al-Askar, A. A. Arishi, F. M. Elkady and A. H. Hashem, *Life*, 2022, **12**, 893.
13 T. J. Matemb Ma Ntep, V. K. Gramm, U. Ruschewitz and C. Janiak, *Chem. Commun.*, 2022, **58**, 8900–8933.
14 K. Kang, S. Liu, M. Zhang, L. Li, C. Liu, L. Lei, X. Dai, C. Xu and C. Xiao, *Adv. Funct. Mater.*, 2022, **32**, 2208148.
15 M. Ding, W. Liu and R. Gref, *Adv. Drug Delivery Rev.*, 2022, **190**, 114496.
16 T. Jia, Y. Gu and F. Li, *J. Environ. Chem. Eng.*, 2022, **10**, 108300.
17 I. Ihsanullah, *Curr. Opin. Environ. Sci. Health*, 2022, **26**, 100335.
18 M. Guo, M. Zhang, R. Liu, X. Zhang and G. Li, *Adv. Sci.*, 2022, **9**, 2103361.
19 D. De and P. Sahoo, *Dalton Trans.*, 2022, **51**, 9950–9965.
20 H. Yuan, N. Li, W. Fan, H. Cai and D. Zhao, *Adv. Sci.*, 2022, **9**, 2104374.

21 I. Hussain, S. Iqbal, C. Lamiel, A. Alfantazi and K. Zhang, *J. Mater. Chem. A*, 2022, **10**, 4475–4488.
22 X. Sun, G. He, C. Xiong, C. Wang, X. Lian, L. Hu, Z. Li, S. J. Dalgarno, Y. W. Yang and J. Tian, *ACS Appl. Mater. Interfaces*, 2021, **13**, 3679–3693.
23 H. Zhao, G. Shu, J. Zhu, Y. Fu, Z. Gu and D. Yang, *Biomaterials*, 2019, **217**, 119332.
24 J. Tang, C. Huang, Y. Liu, T. Wang, M. Yu, H. Hao, W. Zeng, W. Huang, J. Wang and M. Wu, *Coord. Chem. Rev.*, 2023, **490**, 215211.
25 J. Yang, D. Dai, X. Zhang, L. Teng, L. Ma and Y.-W. Yang, *Theranostics*, 2023, **13**, 295–323.
26 M. Wu and Y. Yang, *Adv. Mater.*, 2017, **29**, 1606134.
27 S. Chen, J. Lu, T. You and D. Sun, *Coord. Chem. Rev.*, 2021, **439**, 213929.
28 X. J. Kong, X. Ji, T. He, L. H. Xie, Y. Z. Zhang, H. Lv, C. Ding and J. R. Li, *ACS Appl. Mater. Interfaces*, 2020, **12**, 35375–35384.
29 D. Chakraborty, D. Musib, R. Saha, A. Das, M. K. Raza, V. Ramu, S. Chongdar, K. Sarkar and A. Bhaumik, *Mater. Today Chem.*, 2022, **24**, 100882.
30 W. Zhang, R. Taheri-Ledari, M. Saeidirad, F. S. Qazi, A. Kashtiaray, F. Ganjali, Y. Tian and A. Maleki, *J. Environ. Chem. Eng.*, 2022, **10**, 108836.
31 S. N. Tambat, D. J. Ahirrao, A. B. Pandit, N. Jha and S. M. Sontakke, *Environ. Technol. Innovation*, 2020, **19**, 101021.
32 W. Zhang, Z. Shahnavaz, X. Yan, X. Huang, S. Wu, H. Chen, J. Pan, T. Li and J. Wang, *Inorg. Chem.*, 2022, **61**, 15287–15301.
33 A. Kumar, Y. Kuang, Z. Liang and X. Sun, *Mater. Today Nano*, 2020, **11**, 100076.
34 F. Li, J. Li, L. Zhou and S. Dai, *Sustainable Energy Fuels*, 2021, **5**, 1095–1102.
35 J. Beamish-Cook, K. Shankland, C. A. Murray and P. Vaqueiro, *Cryst. Growth Des.*, 2021, **21**, 3047–3055.
36 V. M. Varsha and G. Nageswaran, *J. Electrochem. Soc.*, 2020, **167**, 155527.
37 J. Y. Tse, K. Kadota, T. Nakajima, H. Uchiyama, S. Tanaka and Y. Tozuka, *Cryst. Growth Des.*, 2022, **22**, 1143–1154.
38 W. Chen, Z. Zhang, L. Hou, C. Yang, H. Shen, K. Yang and Z. Wang, *Sep. Purif. Technol.*, 2020, **250**, 117198.
39 T. Abdullahi, Z. Harun and M. H. D. Othman, *Adv. Powder Technol.*, 2017, **28**, 1827–1840.
40 Y. Hao, H. Guo, F. Yang, J. Zhang, N. Wu, M. Wang, C. Li and W. Yang, *J. Alloys Compd.*, 2022, **911**, 164726.
41 D. Ma, L. Lai, C. P. de León, D. Yuan and J. H. Pan, *Sustainable Mater. Technol.*, 2022, **32**, e00419.
42 Y. Shi, L. Wang, S. Dong, X. Miao, M. Zhang, K. Sun, Y. Zhang, Z. Cao and J. Sun, *Opt. Mater.*, 2022, **131**, 112580.
43 H. Liu, Y. Zhao, C. Zhou, B. Mu and L. Chen, *Chem. Phys. Lett.*, 2021, **780**, 138906.
44 Z. Zhao, H. Li, K. Zhao, L. Wang and X. Gao, *Chem. Eng. J.*, 2022, **428**, 131006.
45 L. Bazzi, I. Ayouch, H. Tachallait and S. EL Hankari, *Results Eng.*, 2022, **13**, 100378.
46 N. Singh, S. Qutub and N. M. Khashab, *J. Mater. Chem. B*, 2021, **9**, 5925–5934.
47 J. Yang and Y. Yang, *Small*, 2020, **16**, 1906846.
48 S. Ullah, M. A. Bustam, A. G. Al-Sehemi, M. A. Assiri, F. A. Abdul Kareem, A. Mukhtar, M. Ayoub and G. Gonfa, *Microporous Mesoporous Mater.*, 2020, **296**, 110002.
49 Y. Liu, Y. K. Lu, B. Zhang, L. Hou and Y. Y. Wang, *Inorg. Chem.*, 2020, **59**, 7531–7538.
50 V. Gupta, S. Mohiyuddin, A. Sachdev, P. K. Soni, P. Gopinath and S. Tyagi, *J. Drug Delivery Sci. Technol.*, 2019, **52**, 846–855.
51 S. H. Paiman, M. A. Rahman, T. Uchikoshi, N. Abdullah, M. H. D. Othman, J. Jaafar, K. H. Abas and A. F. Ismail, *J. Saudi Chem. Soc.*, 2020, **24**, 896–905.
52 M. Moharramnejad, A. Ehsani, M. Shahi, S. Gharanli, H. Saremi, R. E. Malekshah, Z. S. Basmenj, S. Salmani and M. Mohammadi, *J. Drug Delivery Sci. Technol.*, 2023, **81**, 104285.
53 B. Xu, Z. Huang, Y. Liu, S. Li and H. Liu, *Nano Today*, 2023, **48**, 101690.
54 S. F. Fatima, R. Sabouni, R. Garg and H. Gomaa, *Colloids Surf., B*, 2023, **225**, 113266.
55 H. Bunzen and D. Jirák, *ACS Appl. Mater. Interfaces*, 2022, **14**, 50445–50462.
56 H. Xu, S. F. Othman and R. L. Magin, *J. Biosci. Bioeng.*, 2008, **106**, 515–527.
57 J. Yang and Y. Yang, *View*, 2020, **1**, e20.
58 G. Shu, M. Chen, J. Song, X. Xu, C. Lu, Y. Du, M. Xu, Z. Zhao, M. Zhu, K. Fan, X. Fan, S. Fang, B. Tang, Y. Dai, Y. Du and J. Ji, *Bioact. Mater.*, 2021, **6**, 1423–1435.
59 G. J. Soufi, A. Hekmatnia, S. Iravani and R. S. Varma, *ACS Appl. Nano Mater.*, 2022, **5**, 10151–10166.
60 M. Jia, X. Yang, Y. Chen, M. He, W. Zhou, J. Lin, L. An and S. Yang, *J. Mater. Chem. B*, 2021, **9**, 8631–8638.
61 Y. Zhu, N. Xin, Z. Qiao, S. Chen, L. Zeng, Y. Zhang, D. Wei, J. Sun and H. Fan, *Adv. Healthcare Mater.*, 2020, **9**, 2000205.
62 P. Pandit, S. Bhagat, P. Rananaware, Z. Mohanta, M. Kumar, V. Tiwari, S. Singh and V. P. Brahmkhatri, *Microporous Mesoporous Mater.*, 2022, **340**, 112008.
63 Q. You, K. Zhang, J. Liu, C. Liu, H. Wang, M. Wang, S. Ye, H. Gao, L. Lv, C. Wang, L. Zhu and Y. Yang, *Adv. Sci.*, 2020, **7**, 1903341.
64 J. Bao, X. Zu, X. Wang, J. Li, D. Fan, Y. Shi, Q. Xia and J. Cheng, *Int. J. Nanomed.*, 2020, **15**, 7687–7702.
65 X. Zhang, Y. Lu, D. Jia, W. Qiu, X. Ma, X. Zhang, Z. Xu and F. Wen, *J. Nanobiotechnol.*, 2021, **19**, 455.
66 Y. Pu, Y. Zhu, Z. Qiao, N. Xin, S. Chen, J. Sun, R. Jin, Y. Nie and H. Fan, *J. Mater. Chem. B*, 2021, **9**, 1846–1857.
67 A. K. Ghanem and M. J. Budoff, in *Textbook of Arterial Stiffness and Pulsatile Hemodynamics in Health and Disease*, Elsevier, 2022, pp. 77–90.
68 M. Almurayshid, Y. Alssalim, F. Aksouh, R. Almsalam, M. ALQahtani, M. I. Sayyed and F. Almasoud, *Materials*, 2021, **14**, 4957.
69 Y. Ma, J. Mao, H. Qin, P. Liang, W. Huang, C. Liu and J. Gao, *Front. Bioeng. Biotechnol.*, 2022, **10**, 927461.

70 H. Kang, M.-W. Kang, S. Kashiwagi and H. S. Choi, *J. Immunother. Cancer*, 2022, **10**, e004936.
71 H. Nakanotani, Y. Tsuchiya and C. Adachi, *Chem. Lett.*, 2021, **50**, 938–948.
72 Y.-M. Wang, Y. Xu, X. Zhang, Y. Cui, Q. Liang, C. Liu, X. Wang, S. Wu and R. Yang, *Nanomaterials*, 2022, **12**, 287.
73 C. Yuan, Y. Li, Z. Xu, C. Wang, J. Zhang, Y. Jin, Z. Chen, H. Sun, F. Wu, Q. Zhang, Y. Tang and S. Wang, *ACS Appl. Nano Mater.*, 2022, **5**, 15318–15327.
74 L. Li, Z. Qi, S. Han, X. Li, B. Liu and Y. Liu, *Mini-Rev. Med. Chem.*, 2022, **22**, 2564–2580.
75 S. Zhang, F. Rong, C. Guo, F. Duan, L. He, M. Wang, Z. Zhang, M. Kang and M. Du, *Coord. Chem. Rev.*, 2021, **439**, 213948.
76 K.-N. Chi, Y. Guan, X. Zhang, T. Yang, S. Meng, R. Hu and Y.-H. Yang, *Anal. Chim. Acta*, 2021, **1159**, 338378.
77 Y. Wei, Y. Zhang, J.-S. Chen, C. Mao and B.-K. Jin, *Microchim. Acta*, 2020, **187**, 455.
78 F. Duan, M. Hu, C. Guo, Y. Song, M. Wang, L. He, Z. Zhang, R. Pettinari and L. Zhou, *Chem. Eng. J.*, 2020, **398**, 125452.
79 R. Hao, M. Li, F. Li, D. Sun-Waterhouse and D. Li, *Sci. Total Environ.*, 2022, **841**, 156669.
80 M. Zhang, T. Wang, X. Lin, M. Fan, Y. Zho, N. Li and X. Cui, *Sens. Actuators, B*, 2021, **331**, 129411.
81 H. Wang, W. Chen, Q. Chen, N. Liu, H. Cheng and T. Li, *J. Electroanal. Chem.*, 2021, **897**, 115603.
82 G. Mathew, M. Daniel, K. Peramaiah, M.-R. Ganesh and B. Neppolian, *J. Electroanal. Chem.*, 2022, **914**, 116255.
83 Y. Li, J.-J. Li, Q. Zhang, J.-Y. Zhang, N. Zhang, Y.-Z. Fang, J. Yan and Q. Ke, *Sens. Actuators, B*, 2022, **354**, 131140.
84 W. Huang, Y. Xu, Z. Wang, K. Liao, Y. Zhang and Y. Sun, *Talanta*, 2022, **249**, 123612.
85 C. Lin, Y. Huang, L. Luo, F. Fang, J. Zhang, Z. Xun, Y. Fu, H. Shang, C. Liu and Q. Ou, *Front. Immunol.*, 2022, **13**, 927761.
86 Y. Hou, Y. Lu, X. Zhang and Y. Huang, *Sens. Actuators, B*, 2022, **370**, 132409.
87 L. Shi, Y. Ma, H. Zhang, Y. Tan, L. Zhu, Y. Liu, J. Yin, Q. Chen, D. Yang, Y. Qian and Y. Ma, *Talanta*, 2022, **254**, 124139.
88 S. Gertel, A. Polachek, O. Elkayam and V. Furer, *Autoimmun. Rev.*, 2022, **21**, 103085.
89 T. Karashima, S. Umemoto, T. Kishida, K. Osaka, M. Nakagawa, E. Yoshida, T. Yoshimura, M. Sakaguchi, H. Nishimoto, M. Tai, K. Inoue, M. Seiki, N. Koshikawa and T. Shuin, *Cancer Med.*, 2023, **12**, 2453–2462.
90 X. Qin, Y. Pan, J. Zhang, J. Shen and C. Li, *Talanta*, 2023, **253**, 123684.
91 D. Bahari, B. Babamiri, K. Moradi, A. Salimi and R. Hallaj, *Biosens. Bioelectron.*, 2022, **195**, 113657.
92 S. Biswas, Q. Lan, Y. Xie, X. Sun and Y. Wang, *ACS Appl. Mater. Interfaces*, 2021, **13**, 3295–3302.
93 F. G. Ortega, G. E. Gomez, C. Boni, I. C. García, C. G. Navas, R. F. D'vries, M. P. Molina Vallejos, M. J. Serrano, G. A. Messina, J. E. Hernández and M. A. Fernández-Baldo, *Talanta*, 2023, **251**, 123766.
94 H. Dong, S. Liu, Q. Liu, Y. Li, Z. Xu, Y. Li and Q. Wei, *Anal. Chem.*, 2022, **94**, 12852–12859.
95 Y. Hou, J. Wang, S. Liu, Y. Sun, Y. Dai, C. Luo and X. Wang, *Talanta*, 2023, **253**, 123938.
96 K. Feng, T. Li, C. Ye, X. Gao, X. Yue, S. Ding, Q. Dong, M. Yang, G. Huang and J. Zhang, *J. Dairy Sci.*, 2022, **105**, 2108–2118.
97 Z. Sun, J. Li, Y. Tong, H. Han, Y. Yang, C. Wang, H. Li, L. Du and Y. Jiang, *Anal. Chim. Acta*, 2022, **1221**, 340136.
98 O. Bryzgunova, M. Konoshenko, I. Zaporozhchenko, A. Yakovlev and P. Laktionov, *Diagnostics*, 2021, **11**, 865.
99 A. Thakur, D. C. Parra, P. Motallebnejad, M. Brocchi and H. J. Chen, *Bioact. Mater.*, 2022, **10**, 281–294.
100 M. Negahdary and L. Angnes, *Coord. Chem. Rev.*, 2022, **464**, 214565.
101 R. Yuan, H. K. Li and H. He, *Dalton Trans.*, 2021, **50**, 14091–14104.
102 Y. Jiang, R. Li, W. He, Q. Li, X. Yang, S. Li, W. Bai and Y. Li, *Microchim. Acta*, 2022, **189**, 129.
103 Y. Fan, W. Wu, N. Xie, Y. Huang, H. Wu, J. Zhang, X. Guo, S. Ding and B. Guo, *Biosens. Bioelectron.*, 2023, **219**, 114802.
104 K. Yu, M. Li, H. Chai, Q. Liu, X. Hai, M. Tian, L. Qu, T. Xu, G. Zhang and X. Zhang, *Chem. Eng. J.*, 2023, **451**, 138321.
105 D. R. Schmidt, R. Patel, D. G. Kirsch, C. A. Lewis, M. G. Vander Heiden, J. W. Locasale and C. A. Cancer, *J. Clin.*, 2021, **71**, 333–358.
106 P. Rodriguez-Otero, B. Paiva and J. F. San-Miguel, *Cancer Treat. Rev.*, 2021, **100**, 102284.
107 C. Caseiro, J. N. R. Dias, C. M. G. de Andrade Fontes and P. Bule, *Int. J. Mol. Sci.*, 2022, **23**, 3156.
108 G. K. Ali and K. M. Omer, *Anal. Biochem.*, 2022, **658**, 114928.
109 R. Zheng, B. He, L. Xie, H. Yan, L. Jiang, W. Ren, Z. Suo, Y. Xu, M. Wei and H. Jin, *Anal. Chem.*, 2022, **94**, 12866–12874.
110 M. L. Yola, *Microchim. Acta*, 2021, **188**, 78.
111 Y. Li, M. Hu, X. Huang, M. Wang, L. He, Y. Song, Q. Jia, N. Zhou, Z. Zhang and M. Du, *Sens. Actuators, B*, 2020, **306**, 127608.
112 S. Chen, Y. Xie, X. Guo and D. Sun, *Microchem. J.*, 2022, **181**, 107715.
113 S. K. Hari, A. Gauba, N. Shrivastava, R. M. Tripathi, S. K. Jain and A. K. Pandey, *Drug Delivery Transl. Res.*, 2023, **13**, 135–163.
114 H. Xin and S. Naficy, *Gels*, 2022, **8**, 45.
115 S. Daliran, A. R. Oveisi, Y. Peng, A. López-Magano, M. Khajeh, R. Mas-Ballesté, J. Alemán, R. Luque and H. Garcia, *Chem. Soc. Rev.*, 2022, **51**, 7810–7882.
116 J. Munawar, M. Shahzeb Khan, S. E. Zehra Syeda, S. Nawaz, F. Ahmed Janjhi, H. Ul Haq, E. Ullah Rashid, T. Jesionowski and M. Bilal, *Inorg. Chem. Commun.*, 2022, **147**, 110145.
117 G. Fundueanu, M. Constantin, M. Turtoi, S.-M. Bucatariu, B. Cosman, M. Anghelache, G. Voicu and M. Calin, *Pharmaceutics*, 2022, **14**, 865.
118 X. Tan, D. Liao, C. Rao, L. Zhou, Z. Tan, Y. Pan, A. Singh, A. Kumar, J. Liu and B. Li, *J. Solid State Chem.*, 2022, **314**, 123352.
119 S. Sritharan and N. Sivalingam, *Life Sci.*, 2021, **278**, 119527.

120 S. Mallakpour, E. Nikkhoo and C. M. Hussain, *Coord. Chem. Rev.*, 2022, **451**, 214262.
121 C. Rao, D. Liao, Y. Pan, Y. Zhong, W. Zhang, Q. Ouyang, A. Nezamzadeh-Ejhieh and J. Liu, *Expert Opin. Drug Delivery*, 2022, **19**, 1183–1202.
122 M. Pooresmaeil and H. Namazi, *Int. J. Pharm.*, 2022, **625**, 122112.
123 Z. Gharehdaghi, R. Rahimi, S. M. Naghib and F. Molaabasi, *J. Iran. Chem. Soc.*, 2022, **19**, 2727–2737.
124 S. Li, X. Shi, H. Wang and L. Xiao, *J. Biomed. Mater. Res., Part B*, 2021, **109**, 841–852.
125 J. Hu, Y. Chen, H. Zhang, Z. Chen, Y. Ling, Y. Yang, X. Liu, Y. Jia and Y. Zhou, *Microporous Mesoporous Mater.*, 2021, **315**, 110900.
126 C. Sethy and C. N. Kundu, *Biomed. Pharmacother.*, 2021, **137**, 111285.
127 N. Very, S. Hardivillé, A. Decourcelle, J. Thévenet, M. Djouina, A. Page, G. Vergoten, C. Schulz, J. Kerr-Conte, T. Lefebvre, V. Dehennaut and I. El Yazidi-Belkoura, *Oncogene*, 2022, **41**, 745–756.
128 I. Abánades Lázaro, C. J. R. Wells and R. S. Forgan, *Angew. Chem., Int. Ed.*, 2020, **59**, 5211–5217.
129 M. Pooresmaeil, E. A. Asl and H. Namazi, *J. Alloys Compd.*, 2021, **885**, 160992.
130 E. Aghazadeh Asl, M. Pooresmaeil and H. Namazi, *Mater. Chem. Phys.*, 2023, **293**, 126933.
131 R. Jatyan, P. Singh, D. K. Sahel, Y. G. Karthik, A. Mittal and D. Chitkara, *J. Controlled Release*, 2022, **350**, 494–513.
132 Q. Gao, J. Feng, W. Liu, C. Wen, Y. Wu, Q. Liao, L. Zou, X. Sui, T. Xie, J. Zhang and Y. Hu, *Adv. Drug Delivery Rev.*, 2022, **188**, 114445.
133 A. Bazzazzadeh, B. F. Dizaji, N. Kianinejad, A. Nouri and M. Irani, *Int. J. Pharm.*, 2020, **587**, 119674.
134 Z. Wan, C. Li, J. Gu, J. Qian, J. Zhu, J. Wang, Y. Li, J. Jiang, H. Chen and C. Luo, *Int. J. Nanomed.*, 2021, **16**, 6905–6922.
135 T. Kim, H. J. Kim, W. Choi, Y. M. Lee, J. H. Pyo, J. Lee, J. Kim, J. Kim, J.-H. Kim, C. Kim and W. J. Kim, *Nat. Biomed. Eng.*, 2022, **7**, 149–163.
136 A. Cammalleri, P. Croce, W. Lee, K. Yoon and S. S. Yoo, *J. Clin. Neurophysiol.*, 2020, **37**, 104–117.
137 R. C. Alves, Z. M. Schulte, M. T. Luiz, P. Bento Da Silva, R. C. G. Frem, N. L. Rosi and M. Chorilli, *Inorg. Chem.*, 2021, **60**, 11739–11744.
138 V. Zoi, V. Galani, G. D. Lianos, S. Voulgaris, A. P. Kyritsis and G. A. Alexiou, *Biomedicines*, 2021, **9**, 1086.
139 J. Hu, Y. Chen, H. Zhang and Z. Chen, *J. Solid State Chem.*, 2021, **294**, 121853.
140 K. K. Hussain, N. G. Gurudatt, M. H. Akhtar, K.-D. Seo, D.-S. Park and Y.-B. Shim, *Biosens. Bioelectron.*, 2020, **155**, 112094.
141 R. A. Marson Armando, M. P. Abuçafy, A. E. Graminha, R. S. da Silva and R. C. G. Frem, *J. Solid State Chem.*, 2021, **297**, 122081.
142 P. Raju, K. Balakrishnan, M. Mishra, T. Ramasamy and S. Natarajan, *J. Drug Delivery Sci. Technol.*, 2022, **70**, 103223.
143 Y. Lin, X. Qi, H. Liu, K. Xue, S. Xu and Z. Tian, *Cancer Cell Int.*, 2020, **20**, 154.
144 B. Khodashenas, M. Ardjmand, A. S. Rad and M. R. Esfahani, *Mater. Today Chem.*, 2021, **20**, 100474.
145 B. N. Cronstein and T. M. Aune, *Nat. Rev. Rheumatol.*, 2020, **16**, 145–154.
146 Z. Khatibi, N. M. Kazemi and S. Khaleghi, *J. Drug Delivery Sci. Technol.*, 2022, **73**, 103441.
147 K. R. Mazarura, P. Kumar and Y. E. Choonara, *Expert Opin. Drug Delivery*, 2022, **19**, 1149–1163.
148 G. Fang and B. Tang, *Asian J. Pharm. Sci.*, 2020, **15**, 449–460.
149 Q. Ramadan, R. S. Fardous, R. Hazaymeh, S. Alshmmari and M. Zourob, *Adv. Biol.*, 2021, **5**, 2100775.
150 A. Ashkar, A. Sosnik and M. Davidovich-Pinhas, *Biotechnol. Adv.*, 2022, **54**, 107789.
151 H. Bunzen, *ChemNanoMat*, 2021, **7**, 998–1007.
152 E. Moumen, A. H. Assen, K. Adil and Y. Belmabkhout, *Coord. Chem. Rev.*, 2021, **443**, 214020.
153 Y. Wang, J. Yan, N. Wen, H. Xiong, S. Cai, Q. He, Y. Hu, D. Peng, Z. Liu and Y. Liu, *Biomaterials*, 2020, **230**, 119619.
154 D. Wang, L. Xu, F. Yang, Z. Wang, H. Sun, X. Chen, H. Xie and Y. Li, *Ann. Thorac. Surg.*, 2021, **112**, 473–480.
155 N. Qiu, X. Du, J. Ji and G. Zhai, *Drug Dev. Ind. Pharm.*, 2021, **47**, 839–856.
156 J. Liu, P. Leng and Y. Liu, *Fundam. Clin. Pharmacol.*, 2021, **35**, 86–96.
157 X. Lin, L. Miao, X. Wang and H. Tian, *Colloids Surf., B*, 2020, **195**, 111200.
158 P. K. Kalambate, J. Noiphung, N. Rodthongkum, N. Larpant, P. Thirabowonkitphithan, T. Rojanarata, M. Hasan, Y. Huang and W. Laiwattanapaisal, *TrAC, Trends Anal. Chem.*, 2021, **143**, 116403.
159 P. Horcajada, C. Serre, M. Vallet-Regí, M. Sebban, F. Taulelle and G. Férey, *Angew. Chem.*, 2006, **118**, 6120–6124.
160 S. Wang, X. Yang, W. Lu, N. Jiang, G. Zhang, Z. Cheng and W. Liu, *J. Drug Delivery Sci. Technol.*, 2021, **64**, 102593.
161 S. Ohsaki, H. Satsuma, H. Nakamura and S. Watano, *J. Drug Delivery Sci. Technol.*, 2021, **63**, 102490.
162 Y. Wang, W. Lin, S. Yu, X. Huang, X. Lang, Q. He, L. Gao, H. Zhu and J. Chen, *J. Solid State Chem.*, 2021, **293**, 121805.
163 S. Gautam, J. Singhal, H. K. Lee and K. H. Chae, *Mater. Today Chem.*, 2022, **23**, 100647.
164 Z. Yang, D. J. McClements, C. Li, S. Sang, L. Chen, J. Long, C. Qiu and Z. Jin, *Food Hydrocolloids*, 2023, **134**, 108013.
165 S. Singh and A. Goyal, *Emerg. Modalities Mitig. Antimicrob. Resist.*, 2022, 47–78.
166 M. Ebratkhahan, M. Zarei and N. Arsalani, *Sep. Purif. Technol.*, 2022, **299**, 121663.
167 A. Rusu and E. L. Buta, *Pharmaceutics*, 2021, **13**, 2085.
168 Y. Wei, C. Chen, S. Zhai, M. Tan, J. Zhao, X. Zhu, L. Wang, Q. Liu and T. Dai, *Drug Delivery*, 2021, **28**, 372–379.
169 S. Sanaei-Rad, M. A. Ghasemzadeh and S. M. H. Razavian, *Sci. Rep.*, 2021, **11**, 18734.
170 F. A. T. Alsaaed, H. M. A. El-Lateef, M. M. Khalaf, I. M. A. Mohamed, M. A. Al-Omair and M. Gouda, *Polymers*, 2022, **14**, 3815.
171 M. Shen, J. Zhou, M. Elhadidy, Y. Xianyu, J. Feng, D. Liu and T. Ding, *Ultrason. Sonochem.*, 2022, **86**, 106003.

172 Y. Zhou, L. Liu, Y. Cao, S. Yu, C. He and X. Chen, *ACS Appl. Mater. Interfaces*, 2020, **12**, 22581–22592.
173 Y. He, X. Hou, J. Guo, Z. He, T. Guo, Y. Liu, Y. Zhang, J. Zhang and N. Feng, *Carbohydr. Polym.*, 2020, **235**, 115935.
174 A. Rauf, A. Olatunde, M. Imran, F. A. Alhumaydhi, A. S. M. Aljohani, S. A. Khan, M. S. Uddin, S. Mitra, T. Bin Emran, M. Khayrullin, M. Rebezov, M. A. Kamal and M. A. Shariati, *Phytomedicine*, 2021, **90**, 153647.
175 Y. Zhou, Z. Chen, D. Zhao, D. Li, C. He and X. Chen, *Adv. Mater.*, 2021, **33**, 2102044.
176 K. Jiang, W. Ni, X. Cao, L. Zhang and S. Lin, *Mater. Today Bio*, 2022, **13**, 100180.
177 J. Gandara-Loe, B. E. Souza, A. Missyul, G. Giraldo, J. C. Tan and J. Silvestre-Albero, *ACS Appl. Mater. Interfaces*, 2020, **12**, 30189–30197.
178 S. Rojas, I. Colinet, D. Cunha, T. Hidalgo, F. Salles, C. Serre, N. Guillou and P. Horcajada, *ACS Omega*, 2018, **3**, 2994–3003.
179 Z.-J. Lin, H.-Q. Zheng, Y.-N. Zeng, Y.-L. Wang, J. Chen, G.-J. Cao, J.-F. Gu and B. Chen, *Chem. Eng. J.*, 2019, **378**, 122196.
180 M. Zheng, L. Xu, C. Chen, L. Labiadh, B. Yuan and M.-L. Fu, *Sep. Purif. Technol.*, 2022, **294**, 121187.
181 W. S. Chai, J. Y. Cheun, P. S. Kumar, M. Mubashir, Z. Majeed, F. Banat, S.-H. Ho and P. L. Show, *J. Cleaner Prod.*, 2021, **296**, 126589.
182 R. Way, M. C. Ives, P. Mealy and J. D. Farmer, *Joule*, 2022, **6**, 2057–2082.
183 Y. Peng, J. Xu, J. Xu, J. Ma, Y. Bai, S. Cao, S. Zhang and H. Pang, *Adv. Colloid Interface Sci.*, 2022, **307**, 102732.
184 A. Knebel and J. Caro, *Nat. Nanotechnol.*, 2022, **17**, 911–923.
185 T. Wang, E. Lin, Y.-L. Peng, Y. Chen, P. Cheng and Z. Zhang, *Coord. Chem. Rev.*, 2020, **423**, 213485.
186 W. Shang, L. Peng, P. Guo, H. Hui, X. Yang and J. Tian, *ACS Biomater. Sci. Eng.*, 2020, **6**, 1008–1016.
187 K. Böll, A. Zimpel, O. Dietrich, S. Wuttke and M. Peller, *Adv. Ther.*, 2020, **3**, 1900126.
188 Z. Meng, H. Huang, D. Huang, F. Zhang and P. Mi, *J. Colloid Interface Sci.*, 2021, **581**, 31–43.
189 H. Zou, X. Li, W. Zheng and X. Zhou, *Biochem. Biophys. Res. Commun.*, 2022, **608**, 116–121.
190 H. Alijani, A. Noori, N. Faridi, S. Z. Bathaie and M. F. Mousavi, *J. Solid State Chem.*, 2020, **292**, 121680.
191 W. Zhou, J. Shen, J. Lin, M. An, L. An, Q. Tian and S. Yang, *J. Mater. Sci.*, 2021, **56**, 7386–7396.
192 Q. L. Guan, C. Han, F. Y. Bai, J. Liu, Y. H. Xing, Z. Shi and L. X. Sun, *Sens. Actuators, B*, 2020, **325**, 128767.
193 Y. ping Wei, Y. wen Zhang, J. S. Chen, C. jie Mao and B. K. Jin, *Microchim. Acta*, 2020, **187**, 455.
194 S. Akhter, N. K. Mohd Zain, M. Shalauddin, V. K. Singh, I. I. Misnon, R. K. Sharma, S. Das, W. J. Basirun, M. R. Johan and R. Jose, *Sens. Actuators, A*, 2021, **325**, 112711.
195 H. Liang, C. Chen, J. Zeng, M. Zhou, L. Wang, G. Ning, Q. Duan, R. Han, H. Liu, H. Zhao and C.-P. Li, *ACS Appl. Nano Mater.*, 2022, **5**, 16774–16783.
196 Y. B. Miao, Q. Zhong and H. X. Ren, *Anal. Bioanal. Chem.*, 2022, **414**, 8331–8339.
197 X. Shi, Y. Xie, L. Chen, J. Lu, L. Zhang and D. Sun, *Bioelectrochemistry*, 2022, **149**, 108278.
198 N. Rabiee, M. Bagherzadeh, M. Jouyandeh, P. Zarrintaj, M. R. Saeb, M. Mozafari, M. Shokouhimehr and R. S. Varma, *ACS Appl. Bio Mater.*, 2021, **4**, 5106–5121.
199 M. Pooresmaeil and H. Namazi, *J. Taiwan Inst. Chem. Eng.*, 2022, **141**, 104573.
200 S. Yang, Z. Zhao, Y. Xie, J. Lin, B. Zhang and J. Fan, *Int. J. Pharm.*, 2022, **623**, 121912.
201 Q. Jia, Z. Li, C. Guo, X. Huang, Y. Song, N. Zhou, M. Wang, Z. Zhang, L. He and M. Du, *Nanoscale*, 2019, **11**, 20956–20967.
202 Y. Hassanpouraghdam, M. Pooresmaeil and H. Namazi, *Int. J. Biol. Macromol.*, 2022, **221**, 256–267.
203 J. Li, F. Lu, X. Shao and B. You, *Ann. Transl. Med.*, 2021, **9**, 1761.
204 S. Javanbakht, M. Pooresmaeil, H. Hashemi and H. Namazi, *Int. J. Biol. Macromol.*, 2018, **119**, 588–596.
205 M. Mohebi Forouzan, M. A. Ghasemzadeh and S. M. H. Razavian, *Inorg. Nano-Met. Chem.*, 2022, **52**, 1318–1324.
206 M. Gao, C. Yang, C. Wu, Y. Chen, H. Zhuang, J. Wang and Z. Cao, *J. Nanobiotechnol.*, 2022, **20**, 404.
207 A. Botet-Carreras, C. Tamames-Tabar, F. Salles, S. Rojas, E. Imbuluzqueta, H. Lana, M. J. Blanco-Prieto and P. Horcajada, *J. Mater. Chem. B*, 2021, **9**, 2233–2239.
208 A. P. Acharya, K. B. Sezginel, H. P. Gideon, A. C. Greene, H. D. Lawson, S. Inamdar, Y. Tang, A. J. Fraser, K. V. Patel, C. Liu, N. L. Rosi, S. Y. Chan, J. A. L. Flynn, C. E. Wilmer and S. R. Little, *J. Controlled Release*, 2022, **352**, 242–255.
209 P. B. So, H. T. Chen and C. H. Lin, *Microporous Mesoporous Mater.*, 2020, **309**, 110495.